2012-04-09

Simulations of Controlled Fires Using the One-Dimensional Turbulence Model with Application to Fire Spread in Wildland Fires

Elizabeth Ida Monson
Brigham Young University - Provo

Simulations of Controlled Fires Using the One-Dimensional Turbulence Model

with Application to Fire Spread in Wildland Fires

Elizabeth I. Monson

A thesis submitted to the faculty of
Brigham Young University
in partial fulfillment of the requirements for the degree of

Master of Science

David O. Lignell, Chair
Thomas H. Fletcher
Bradley C. Bundy

Department of Chemical Engineering

Brigham Young University

June 2012

ABSTRACT

Simulations of Controlled Fires Using the One-Dimensional Turbulence Model
with Application to Fire Spread in Wildland Fires

Elizabeth I. Monson
Department of Chemical Engineering, BYU
Master of Science

The mechanism of flame propagation in fuel beds of wildland fires is important to understand and quantify fire spread rates. Fires spread by radiative and convective heating and often require direct flame contact to achieve ignition. The flame interface in an advancing fire is unsteady and turbulent, making study of intermittent flames in complex fuels difficult. This thesis applies the one-dimensional turbulence (ODT) model to a study of flame propagation by simulating a lab-scale fire representative of the flame interface in a fuel bed and incorporating solid fuel particles into the ODT code. The ODT model is able to resolve individual flames (a unique property of this model) and provide realistic turbulent statistics. ODT solves diffusion-reaction equations on a line-of-sight that is advanced either in time or in one spatial direction (perpendicular to the line-of-sight). Turbulent advection is modeled through stochastic domain mapping processes.

A vertical wall fire, in which ethylene fuel is slowly fed through a porous ceramic, is modeled to investigate an unsteady turbulent flame front in a controlled environment. Simulations of this configuration are performed using a spatial formulation of the ODT model, where the ODT line is perpendicular to the wall and is advanced up the wall. Simulations include radiation and soot effects and are compared to experimental temperature data taken over a range of fuel flow rates. Flame structure, velocities, and temperature statistics are reported. The ODT model is shown to capture the evolution of the flame and describe the intermittent properties at the flame edge, though temperature fluctuations are somewhat over predicted.

A solid particle devolatilization model was included in the ODT code to study the convective heating of unburnt solid fuels through direct flame contact. Here the particles are treated as sweet gum hardwood and a single-reaction, first order decomposition model is used to simulate the devolatilization rates. Only preliminary results were presented for a simple case, but this extension of the ODT model presents new opportunities for future research.

Keywords: one-dimensional turbulence, turbulence, wall fire, ethylene fire, fire propagation, particle devolatilization

ACKNOWLEDGMENTS

There are many people who have helped me to complete this project. First, I wish to thank Dr. David Lignell who provided constructive feedback and help with this project. I would also like to thank the other members of my committee: Dr. Thomas Fletcher and Dr. Bradley Bundy for their input and insight. I am also grateful for Ryan Hintze, an undergraduate student, for the time that he spent on this project. I am thankful for the USDA Forest Service Rocky Mountain Research Station for providing financial support.

Lastly, I wish to thank my husband, Jake Monson, and my parents, John and Barbara Haake, for their constant support and encouragement.

TABLE OF CONTENTS

LIST OF TABLES

LIST OF FIGURES

NOMENCLATURE

A	Particle surface area
a	Amplitude parameter in log normal distribution
α	Width parameter in log normal distribution
β	ODT scaling parameter
C	ODT scaling parameter
C_{min}	Number of nucleated carbon atoms
c	Arbitrary constant value
χ	Fraction of solid particle grid cell that overlaps gas phase grid cell
D	Diffusivity
D_p	Diameter of a particle
Δt	Temporal or spatial advancement increment of an eddy
Δx	ODT cell size
δ_m	Momentum boundary layer thickness
δ_T	Temperature boundary layer thickness
E	Activation energy
E_{kin}	Eddy kinetic energy
e	Internal energy of the ODT system
η	Arbitrary conservation property per unit mass
$\vec{F}_{ext}$	External force on the ODT system
f	Frequency
$f(x)$	Eddy triplet map as function
f_v	Soot volume fraction
γ	Volume fraction of gas phase to total fraction (i.e. void fraction)
h	Enthalpy
I	Radiative intensity
j	Diffusion flux
k	Rate constant
k_0	Pre-exponential factor
k_b	Boltzmann constant
κ	Absorption coefficient
L	Domain length
l_E	Eddy size
λ_E	Eddy rate, defined by the kinetic energy of the eddy
λ	Thermal conductivity
m_p	Mass per volume of grid cell
μ_s	Skewness parameter in log normal distribution
μ	Dynamic viscosity
MW	Molecular weight
n	Number density
Na	Avogadro's number
Nu	Nusselt number
ν	kinematic viscosity
Ω	System being evolved by ODT

ω	Reaction source term
P	Pressure
$P(x_0, l)$	Approximate eddy distribution
P_a	Eddy probability
$\phi(x)$	Map of fluid system in the x domain
Π	Boundary of system being evolved by ODT
Pr	Prandlt number
$\dot{Q}$	Heat added to the ODT system
q	Heat flux
R	Universal gas constant
Re	Reynolds number
ρ	Density
S_n	Soot number density source term
S_Φ	Gas phase mass source term from devolatilization of wood particles
S_{Y_s}	Soot mass fraction source term
σ	RMS fluctuations
σ	Stephan-Boltzmann constant
T	Temperature
t	Time
Θ	Arbitrary scaled property
θ	Blowing factor in heat transfer to a particle
τ_E	Turbulent timescale
τ_o	Optical thickness
τ_{xy}	Viscous stress tensor
u	Streamwise velocity (perpendicular to the ODT line)
V	Volume
v^D	Diffusion velocity
$\vec{v}_{cv}$	ODT control volume velocity
$\vec{v}_{sys}$	ODT system velocity
$\vec{v}_R$	Relative velocity of ODT system
X	Mole fraction of chemical species
$\dot{W}$	Work on the ODT system
x	ODT line direction
x_0	Eddie location
ξ	Mixture fraction
Y	Mass fraction of chemical species
y	Axes normal to the ODT line direction
y_p	Yield of pyrolysis gas
y_p^*	Ultimate pyrolysis yield
Z	ODT scaling parameter

Subscripts, superscripts, and other indicators

$\dot{[\,]}$	indicates [ ] is a rate
$\hat{[\,]}$	indicates [ ] is a Eulerian property
$[\,]^-$	indicates [ ] is in the direction of decreasing x

$[\,]^{+}$	indicates [ ] is in the direction of increasing x
$[\,]_{0}$	indicates [ ] is the initial value or property at x = 0 in the domain
$[\,]_{b}$	indicates [ ] is a black body property
$[\,]_{E}$	indicates [ ] is an eddy property
$[\,]_{e}$	indicates [ ] is from the east face of a grid cell
$[\,]_{f}$	indicates [ ] is a final value
$[\,]_{g}$	indicates [ ] is a gas phase property
$[\,]_{i}$	indicates [ ] is a property of chemical species i or a property of the ith grid cell
$[\,]_{in}$	indicates [ ] is an inlet property at the wall
$[\,]_{\infty}$	indicates [ ] is a property of the surroundings
$[\,]_{L}$	indicates [ ] is the property value at x = L in the domain
$[\,]_{m}$	indicates [ ] is a mean property
$[\,]_{max}$	indicates [ ] is the maximum value
$[\,]_{n}$	indicates [ ] is the nth item in a list or series
$[\,]_{p}$	indicates [ ] is a particle property
$[\,]_{rad}$	indicates [ ] is a radiative property
$[\,]_{s}$	indicates [ ] is a soot property
$[\,]_{w}$	indicates [ ] is from the west face of a grid cell
$[\,]_{w}$	indicates [ ] is a wall property

CHAPTER 1. INTRODUCTION

Wildland fires are responsible for damaging human lives and property, degrading soil, and altering landscapes. Increased knowledge of the physics and properties of these fires are needed to better maintain the environments prone to these fires. Over the past several decades much research has gone into predicting wildland fires to support firefighting and fire prevention methods. Understanding the mechanism of flame propagation in wildland fires is important to develop accurate fire models and predict fire behavior.

A flame front propagates through an unburnt fuel bed by radiative heating from the burning flames and by convective heating by direct flame contact [1]. Although some models have focused on radiation being the main mechanism [2–4], experiments and observations have indicated the importance of direct flame contact [5]. Weber [6] found that the preheating of particles ahead of the flame front in fuel beds could not be accounted for by radiation models. Cohen and Finney [7] demonstrate preferential ignition of large diameter fuels over fine fuels exposed to the same radiative source since convection of surrounding air (induced by buoyant acceleration at the heat source) allows cooling of the fine fuel.

Flame propagation by convective heating of unburnt fuel through flame bathing is a complex process influenced by many factors. The flame front at the interface between burned and unburnt fuel is typically turbulent, with the flow driven by buoyant acceleration in the flame zone and wind effects [8, 9]. Turbulent flames involve a wide range of time and length scales, ranging from sub-millimeter flames to scales as large as the fire itself (tens of meters in forest crown fires). Flames in fuel beds involve many differentially-diffusing species whose identity and chemical mechanisms may be unknown. Soot formation and radiative transport further complicate the process. Hot combustion gases have lower density than surrounding air, which causes expansion. Cumulative expansion of combustion gases causes an incline in the flame front. The propagation of the flame front is unsteady, with intermittent turbulent flames in fuel beds involving complex fuels

and spatial distributions. Excursions of flame into the unburnt fuel region, which are increased by an inclined flame front, have been shown to result directly in fuel ignition and subsequent flame propagation [9].

Computational models are an important tool in better understanding the physics and dynamics of fire propagation via direct flame contact. Development of these models will help improve management techniques such as prescribed burns, thinning of fuels, and risk analysis of property in environments prone to wildland fires. These models and their resulting simulations are complementary to experimental investigation and can provide insights that are not feasible to obtain experimentally. However, it should be noted that the reliability of a simulation is only as good as the equations on which it is formulated. Therefore, an understanding of the proper physics is important.

To simulate flame propagation by direct flame contact, the turbulent flame itself must be resolved. The only simulation approach that can resolve flames in turbulent flows is direct numerical simulation (DNS). DNS does not involve turbulence models, but numerically solves the full Navier-Stokes equations. The consequence of the full resolution is the high computational cost. Reynolds-averaged Navier-Stokes (RANS) and large eddy simulation (LES) approaches can capture the larger fire scales, but cannot resolve individual flames. RANS solves the time-averaged Navier-Stokes equations and LES solves the spatially-filtered Navier-Stokes equations. Both RANS and LES are relatively, computationally efficient, but do not resolve all the diffusive and reaction scales. RANS and LES require sub-grid models, which are not directly coupled to evolving diffusive structures.

A relatively new approach is the one-dimensional turbulence model (ODT) [10, 11], which approximates large-scale flow and can resolve individual flames in an efficient and relatively computationally inexpensive way. It does this by reducing the dimensionality of the problem. Reaction-diffusion equations for mass, momentum, species, and energy are solved along a line-of-sight through a given flow. Turbulent advection is modeled in ODT using a stochastic domain remapping processes that simulates the effect of turbulent eddies. ODT is described further in Chapter 3, but the key point is that it is able to resolve individual flames with realistic turbulent statistics.

This thesis uses the ODT model to further the study of flame propagation in wildland fires by:

1. The formulation and implementation of a spatial formulation of ODT.

2. The simulation of an ethylene wall fire was simulated to collect flame front statistics.

3. The implementation of solid wood particle devolitilization into the ODT code.

The primary objectives are: (1) to increase understanding of flame structure and important statistics that describe a flame front, and (2) present ODT as a viable tool in understanding flame propagation in fuel beds. Chapter 2 provides the background of this research. A description of the formulation of the ODT model and the implementation of a spatial formulation into the current code are included in Chapter 3. The application of ODT to the ethylene wall fire along with the results and a comparison to experimental data are provided in Chapter 4. Chapter 5 discusses the introduction of wood particle combustion into a temporal formulation of the current code. Finally, conclusions and opportunities for future research are discussed in Chapter 6.

CHAPTER 2. BACKGROUND

Current simulations of wildland fires focus primarily upon fire spread rates, and provide little insight to the flame structure and flow physics at the flame fuel interface. Several of these models are more empirical in nature. Some use a more physics-based approach by using common turbulence methods, which do not affordably resolve all turbulent scales. The following section provides more detail on the common turbulent methods and examples of their use in simulating fires representative of wildland fires.

2.1 Reynolds Average Navier-Stokes (RANS)

RANS solves the time-averaged Navier-Stokes equations, with turbulence models for unclosed Reynolds stresses. These Reynolds stresses are unknown, and are determined from mean flow components. The process of determining the Reynolds stresses, called closure, cannot be done using a single model for all flows, because no universal closure model exists. Therefore several closure models are tuned and applied for different flows [12].

RANS is commonly used in turbulent combustion modeling because it is computationally faster than most other methods. A large domain simulation can be run on a single processor in a couple of days. However, the accuracy of the flow physics is limited to use in identifying major trends [13]. Examples of RANS-based wildland fire models are IUSTI [14–17] and FIRETEC [18, 19]. Morvan and Larini [20] applied IUSTI to simulate a controlled fire through a pine needle fuel bed, with good agreement to experimental results. Applicable to the wall fire in this research (described further in the wall fire review of this chapter) are several wall fire cases that use a RANS method [21–23].

2.2 Large Eddy Simulation

LES applies a spatial filter to the Navier-Stokes equations, rather than the temporal filter used in RANS, hence removing small scales. Therefore, LES is used to model the transient nature of the larger, energy containing eddies. This filtering process introduces additional terms, analogous to Reynolds stresses that must be closed. Similar to RANS, there are closure models for LES. The advantage of LES to RANS is that these closure models are not as dependent upon flow configuration [12].

LES is becoming more common in combustion modeling [24], and can be seen as an intermediate between RANS and DNS [13]. The computational costs are much higher in LES than RANS. LES does not resolve the small turbulent scales necessary to accurately describe flamelets and flame fluctuations. Few attempts have been made to apply LES to wildland fires due to the computational costs associated with this method. Zhou et al. [25] used LES to simulate laboratory-scale fire spread in live chaparral fuel beds, in order to study the effect of slope on flame propagation. A study of buoyancy-driven wall fires was performed by Wang et al. [26], which is discussed further in the review of wall fires.

2.3 Direct Numerical Simulation

Direct numerical simulation is a direct application of the fully-compressible Navier-Stokes equations, thus no model for turbulence is necessary. This results in a high level of numerical fidelity. DNS has the advantage that it resolves all turbulent length and time scales. In order to resolve all these length and time scales, a fine grid and small time steps must be applied. This results in very high computational costs. For example, a simulation of a hydrogen jet flame with a centimeter-scale domain, and a millisecond run time, requires about 3.5 million CPU-hours running for 10 days on about 10,000 processors [27].

Due to high computational cost, DNS in combustion modeling is limited to small-scale, canonical flows. It is often used to validate other turbulence models [12]. DNS has proved to be a powerful tool in understanding turbulent combustion [13], but is not practical for typical fire modeling.

2.4 The Linear Eddy Model

Kerstein developed the Linear Eddy Model (LEM) [28] as a turbulence model which treats turbulent stirring and molecular diffusion separately. Turbulent mixing is treated stochastically rather than using an equation of evolution. It is stochastic, because the times and sizes of eddies are sampled randomly from a predefined eddy distribution function. The turbulent strain and rotational folding effects of eddies are represented through a process called triplet mapping. Triplet mapping is the simulation of an eddy by instantaneously mapping a segment of a one-dimensional domain onto itself. Molecular diffusion is carried out through the numerical time integration of a Fickian diffusion equation along a one-dimensional domain.

LEM has been applied to many flows including: turbulent shear layers [28, 29], the microstructure of diffusive scalar mixing [30], finite-rate chemistry and multi-stream mixing [31]. It has not been applied to wildland fires or fuel beds.

2.5 One Dimensional Turbulence

One-dimensional turbulence (ODT) was developed as an extension to LEM [18]. The ODT model treats turbulent advection and molecular diffusion similarly to the LEM model. However, the ODT model has the advantage in that the eddy distribution function is not predetermined but advances in time and is calculated from the local, instantaneous velocity field. Turbulence is assumed to be homogeneous in LEM, while ODT is more general in its treatment of turbulence. Another advantage it that ODT evolves a velocity field and can account for turbulent intensity variations with local shear profiles.

Several applications of ODT to turbulent flows have been performed. These include many studies which have been performed on non-reacting systems: buoyant stratified flows [10], wakes, jets [11], mixing layers [32, 33], LES closure [34–36], deposition of inertial particles [37], vertical slots [38] and isothermal walls [39]. Applying ODT to turbulent, reacting flows is a relatively new approach, therefore only a few studies have been carried out.

Echekki et al. [40] undertook the first application of ODT to a reacting system. This study was a simulation of turbulent jet diffusion flames. Echekki et al. [41] later applied ODT to hydrogen autoignition in a turbulent jet with preheated, co-flowing air. Some research has been com-

pleted involving the prediction of extinction and reignition in turbulent jet diffusion flames using ODT. Hewson et al. [42] developed a simulation of local extinction and reignition in non-premixed turbulent $CO/H_2/N_2$ jet flames. Later studies, performed by Ranganath and Echekki [43,44], generated more general extinction and reignition turbulent jet diffusion models. These results were in reasonable agreement with experimental results. The authors suggest that this model may be difficult to apply to more complicated flow configurations. Ricks et al. [45] conducted a study of soot and enthalpy evolution in meter-scale buoyant fires by using ODT. Shihn and DesJardin [46] applied a temporal and a simplified spatial formulation of ODT to a vertical wall fire, which will be discussed more in the following section.

2.6 Review of Wall Fire Studies

Many studies about turbulent natural convection fires on vertical walls and vertical gas-panel burners have been conducted with the motivation of improving the understanding of the spreading of wall fires. These include several experimental studies and some modeling. Most of the available models are either empirical or analytical methods. Only one study gives insights into the variable flame structure along the flame front, but still does not capture all the relevant scales [26].

Several experimental studies have been performed on solid and gas panel wall fires. De Ris and Orloff [47] studied radiation effects on pool, wall and ceiling fires. The experiments were carried out on a sintered metal gas burner. The main focus of their work was the effect of orientation on the flames. Radiant heat flux and burning rates were reported for the various orientations. Orloff et al. [48] studied heat transfer, burning rates, and flame spread velocities of thermally thick polymethyl methacrylate (PMMA) slabs. Later they went on to include burning rates and radiance in their study [49]. Flame heights and radiation in solid burning walls were studied by King-Mom and Quintiere [50] for PMMA and douglas fir particle board. Marksein and De Ris [51] studied radiation and heat transfer from gas panel burners.

A few empirical models were used in the study of wall fires. An empirical model, developed by Quintiere [52], was used to predict upward flame spread in a room. Also, Mitler [53] developed a semi empirical model for the prediction of fire spread rates on vertical PMMA slabs. The results were compared to experimental data with good agreement.

Delichatsios [54, 55] created a simple two-layer integral model for buoyancy driven wall flows, which includes two turbulent layers (one near the wall and the other farther out). The properties are matched at the interface between the two layers. This was applied to both non-reacting and burning wall flows (ethane, ethanol, methanol, and PMMA fuels). These studies focused on flame heights (the distance from the base of the wall to the top of the fire), flame intensities, and burning/pyrolysis rates. These results were compared to experimental pyrolysis/burning rates and velocities. A simple algebraic model for wall fires, which was based on the two-layer model was also developed [56], and compared to the same experimental results.

Some modeling methods applied to wall fires employ more physical models. Kennedy and Plumb [21] were the first to apply a time averaged k-ε-g model to both an inert, turbulent, vertical-wall flow and a burning wall case. The model reported mean and RMS values for temperature and fuel fraction and burning rates. Comparison to experimental results were made for the inert wall with good agreement. A simplified chemistry model was used for the burning wall. Tamanini [22] also used a modified k-ε-g model to simulate wall fire spread in a room. Later, another study by Joulain [23] applied the k-ε-g model to both vertical gas panel burners and vertical solid burning walls (for various gaseous and solid fuels). Burning rates, mean velocities, mean temperatures, and turbulence intensities were reported and compared to their experimental data (experimental and modeling studies were carried out in this work), and showed good agreement. While the k-ε-g model involves more flow physics than many other modeling methods employed for wall fires, it is a time averaging method and not all relevant time and length scales are resolved in these studies.

Wang et al. [26] used LES to investigate the transport characteristics and flame structures of vertical wall fires. A simplified chemistry approach was taken in this study, where chemical reactions were assumed to be infinitely fast. Mean flame heights, and temperature and velocity profiles were reported and compared to experimental data with good agreement. LES is a filtered model and the small scales are not resolved in this approach. An empirical model was used for the subgrid scale.

2.7 Summary

There has been extensive research in the area of fire spread in wildland fuel beds, both experimental and theoretical. Much of this research focuses on radiation as being the most im-

portant and in some cases only mechanism for flame propagation. Recently, the importance of flame spread via direct flame contact has been noted [7]. This requires a better knowledge of flame structure and flow physics at a flame edge. Modeling and simulations provide a better physical understanding of the flame front. Several turbulence modeling methods can and have been employed to lab scale fires to acquire flame statistics. However, these can be computationally expensive and most still do not resolve the time and length scales involved at a flame edge. The need for a model that is capable of full resolution is needed. The ODT model is a good model for this purpose.

Wall fires are studied, because they provide a simplified fuel and configuration that is amenable to experimental investigation and model validation. The statistics in these fires are representative to those found in in a flame front in a fuel bed. Many studies have been done on wall fires. These studies focused more on burning/pyrolyzing rates, flame heights on the wall, and flame spread rates along the wall. Only Wang et al. focused on the flame structure of the fires, but a LES model was used which cannot resolve the small scales that are present in these fires. Therefore, more research is needed to obtain an understanding of the flame structure and flow physics of a wall fire.

CHAPTER 3. ONE DIMENSIONAL TURBULENCE

The ODT code used in this research is written in C++ and has been under development for the last four years. The code has two formulations: (1) temporal, which evolves all processes with time, and (2) spatial, which advances the processes in a spatial direction perpendicular to the ODT line by using boundary layer assumptions. That is, there is one line of sight through the simulation that advances in time or space.

In the ODT code, reaction-diffusion equations for mass, momentum, energy, and species are solved in their conservative form along a given line-of-sight in a single evolution dimension (time or spatial direction perpendicular to the line of sight). Stochastic eddy events, accounting for effects of turbulent advection, happen concurrently with evolution of the reactive-diffusive system. This turbulence modeling method is described in more detail later in this chapter.

Since turbulence involves a wide range of time and length scales, full resolution of a turbulent flow at the level of the smallest structures can be costly, even in one dimension. To overcome this, the ODT code employs an adaptive grid, which allows resolution of local velocities and other reactive scalars. The grid adapts in such a way that there are more grid points where there are higher gradients due to turbulence and chemical reactions. This greatly reduces computational costs, because portions of the domain experience high turbulence, while others are relatively smooth.

The diffusive advancement uses a Lagrangian control volume formulation in which cells expand or contract such that the total mass or vertical mass flux (depending on the formulation) is constant in any given cell. Mass conservation is important in combustion systems in which species, energy, and momentum balances dictate the evolution of the flow. Throughout the code, mass conservation is ensured in all steps of the advancement process. For example in the mesh adaption scheme, which involves the merging and splitting of cells, mass conservation is maintained. All convection along the line occurs through flow dilatation from heat release. Cell faces move at the local velocity, so there is no net mass flux across the cell. Hence, cells expend or contract as

required by continuity. When enforcing mass conservation, it is assumed that the contents of a grid cell are uniform throughout the cell.

Thermochemical and transport properties are implemented using composition, temperature, and pressure dependent functions. The Cantera package [57] is used to compute these functions and as an option for chemical kinetics.

3.1 Turbulent Mixing

The ODT model employs a stochastic method for simulating the turbulent advection in a flow. It is stochastic, because as the code advances for a given space or time (depending on the formulation) eddies are randomly sampled until a feasible eddy is accepted. The process of sampling and accepting an eddy occurs as follows. A candidate eddy has a given location x_0, size l_E, and rate λ_E. The eddy rate is defined by the kinetic energy E_{kin} (form of E_{kin} given in [33]) in the eddy region and scaling parameters C and Z. This definition is

$$\lambda_E = \frac{1}{l_E^2 \tau_E}, \tag{3.1}$$

where τ_E is the turbulent timescale given by:

$$\frac{1}{\tau_E} = C\sqrt{\frac{2}{\rho l_E^3}(E_{kin} - Z\frac{\nu^2}{\rho 2 l_E})}. \tag{3.2}$$

Here ν is the local kinematic viscosity and ρ is the local density. This eddy is sampled from an approximate eddy distribution $P(x_0, l_E)$ at time Δt_s (Δt_s is a spatial advancement increment in the spatial formulation), which is sampled from a Poisson distribution with mean Δt_m. The definition of $P(x_0, l_E)$ is given in [58]. The eddy is accepted with probability:

$$P_a = \Delta t_m \lambda_E / P(x_0, l_E). \tag{3.3}$$

There is also an eddy suppression method used (not described here) which suppresses unrealistically large eddies and includes a third scaling parameter β. This large eddy suppression uses an

elapsed time method where the time of the eddy, t, must follow the constraint

$$t < \beta * \tau_E, \tag{3.4}$$

or it is not accepted. If the eddy is accepted, then a triplet map (described further in the next paragraph) is implemented, and the domain is diffused up to the time or location of the eddy event.

The turbulent strain and rotational folding effects of eddies are represented through a process called triplet mapping. Triplet mapping is the simulation of an eddy by instantaneously mapping a segment of a one-dimensional domain onto itself. The triplet map is implemented by moving fluid at a certain location to another, $\phi(x) \rightarrow \phi(f(x))$. Here $f(x)$, or the map, is defined by:

$$f(x) = \begin{cases} 3(x-x_0) & \text{if } x_0 \leq x \leq x_0 + \frac{1}{3}l_E \\ 2l_E - 3(x-x_0) & \text{if } x_0 + \frac{1}{3}l_E \leq x \leq x_0 + \frac{2}{3}l_E, \\ 3(x-x_0) - 2l_E & \text{if } x_0 + \frac{2}{3}l_E \leq x \leq x_0 + l_E, \\ x - x_0 & \text{otherwise.} \end{cases} \tag{3.5}$$

When the triplet map occurs, profiles in the eddy region are compressed spatially to a third of its original size, and three copies are placed on the original eddy region, with the middle copy inverted. This triplet mapping is illustrated in Figure 3.1. When a triplet map is implemented, properties are conserved, profiles remain continuous, and diffusive mixing increases by increasing scalar gradients. This causes the eddy rate in the eddy region to increase, which accelerates the occurrence of triplet maps. In this way the ODT formulation reproduces characteristic aspects of turbulence, such as the five-thirds energy cascade [12].

3.2 Reactive-Diffusive Mixing

The two ODT formulations have different governing equations for the reactive-diffusive mixing. The temporal formulation is described in this section along with the development of the spatial formulation that has been done for the current study. The spatial formulation of the code was required for simulation of the ethylene wall fire considered in this research effort. A spatial formulation was not available previously and therefore was implemented into the existing ODT code.

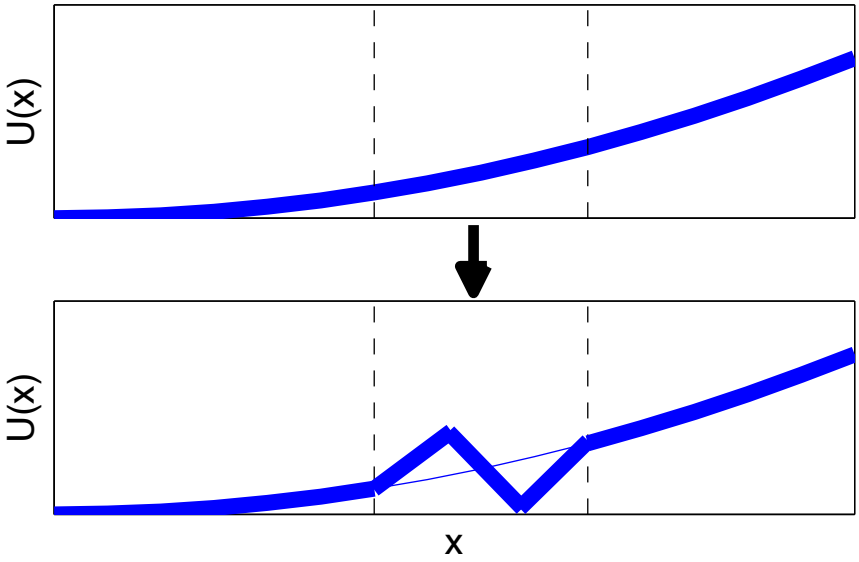

Figure 3.1: Illustration of a triplet map.

Also, note the absence of a convective term in both the spatial and temporal ODT formulations. Convection (up to a constant) arises only through dilatation (density variation), which, for low-Mach flows, occurs due to heat release. The Lagrangian formulation accounts for these changes through changes in the grid size.

3.2.1 Temporal Formulation

In this formulation the governing equations are advanced in time along the ODT line of sight. Therefore, the temporal formulation is well suited for turbulent flows that are homogeneous in the streamwise direction (perpendicular to the ODT line).

The constraint for continuity applied to the grid control volumes is

$$\rho \Delta x = c, \tag{3.6}$$

where ρ is density, Δx is cell width, and c is a constant. This means that the mass is conserved in grid cells. The diffusive advancement occurs using scalar equations for momentum, energy, and chemical species, derived from the Reynolds transport theorem. These governing equations are

given by:

$$\text{momentum: } \frac{\partial u}{\partial t} = -\frac{\tau_{xy,e} - \tau_{xy,w}}{\rho \Delta x} - \frac{1}{\rho}\frac{\partial P}{\partial y}, \tag{3.7}$$

$$\text{chemical species: } \frac{\partial Y_i}{\partial t} = -\frac{j_e - j_w}{\rho \Delta x} + \frac{\omega_i}{\rho}, \tag{3.8}$$

$$\text{energy: } \frac{\partial h}{\partial t} = \frac{1}{\rho}\frac{\partial P}{\partial t} - \frac{q_e - q_w}{\rho \Delta x}. \tag{3.9}$$

In these equations t is the time, ρ is the density, x is the line direction, y is the direction perpendicular to the line, Δx is the cell size, P is the pressure, u is the stream-wise velocity (in the y direction), τ is the viscous stress tensor, q is the heat flux, j is the diffusion flux, ω is the reaction source term, and C_p and C_v are the constant pressure and volume mixture heat capacities. Here the subscripts e and w indicate the east and west faces of a cell, respectively. The subscript i indicates species i.

The stress tensor used in the momentum equation is defined as

$$\tau_{yx} = -\mu \frac{\partial u}{\partial x}, \tag{3.10}$$

where μ is the local viscosity. Fick's law is used to define the species flux as:

$$j_i = \rho Y_i v_i^D = -\frac{\rho Y_i D_i}{X_i}\frac{\partial X_i}{\partial x} = -\rho D_i \frac{\partial Y_i}{\partial x} - \frac{\rho D_i Y_i}{MW}\frac{\partial MW}{\partial x}. \tag{3.11}$$

Here D_i is the diffusion coefficient, and X_i is the mole fraction. The heat flux includes thermal conduction, species mass flux, and radiative flux terms and is defined by:

$$q = -\lambda \frac{\partial T}{\partial x} + \sum_i h_i j_i + q_{rad}, \tag{3.12}$$

where h_i is the species enthalpy, λ is the thermal conductivity, q_{rad} is the radiative flux (discussed in more detail in the radiation model section), and T is the temperature. The derivatives in all the flux terms are evaluated at the cell faces using a central difference method.

3.2.2 Spatial Formulation

The spatial formulation of the code was developed and implemented in this research. This formulation is similar to that reported in [33]. Unlike the temporal formulation, the spatial formulation models turbulent flows that are not homogeneous in the streamwise direction. It allows flows which are two-dimensional in nature. This allows many more flow configurations to be modeled. Since the spatial formation is still one dimensional it is parabolic in nature and a marching method still must be used. Therefore, the spatial formulation assumes basic boundary layer assumptions. This means that the streamwise velocity component dominates over other velocity components. Also, gradients are strongest along the ODT line with negligible diffusion in the streamwise direction. The diffusive-reactive system is advanced as if the flow were steady, but instantaneous rearrangements occur due to the eddy events.

The spatial formulation is similar to the temporal formulation, so the symbols in this section have similar definitions to those given in the temporal formulation. The diffusive advancement equations for this formulation were also derived using the Reynolds transport theorem, but unlike the temporal formulation, standard boundary layer assumptions were also applied. The constraint for continuity across the Lagrangian grid is $\rho u \Delta x = c$. So, the main difference between these formulations is that the mass flux is conserved in the spatial formulation rather than the mass. The governing equations for the spatial formulation are given by:

$$\text{momentum: } \frac{\partial u}{\partial y} = -\frac{\tau_{xy,e} - \tau_{xy,w}}{\rho u \Delta x} - \frac{1}{\rho u}\frac{\partial P}{\partial y}, \tag{3.13}$$

$$\text{chemical species: } \frac{\partial Y_i}{\partial y} = -\frac{j_e - j_w}{\rho u \Delta x} + \frac{\omega_i}{\rho u}, \tag{3.14}$$

$$\text{energy: } \frac{\partial h}{\partial y} = \frac{1}{\rho u}\frac{\partial P}{\partial t} - \frac{q_e - q_w}{\rho u \Delta x}. \tag{3.15}$$

Here all scalar transport equations are divided by the velocity, which prohibits the velocity from ever being equal or less than zero. These scalar transport rates diverge when the velocity is zero.

Mechanics of Merging Cells

Since the grid is adaptive while evolving, there are several places in the code where cells need to be merged. It is important to obey conservation laws when merging cells in an adaptive

grid. For the spatial case this is slightly more complex, because the spatial case conserves mass flux rather than mass. Therefore, density and velocity are coupled and require more steps to obtain their separate values.

Several cells are merged by starting with the mass flux conservation equation:

$$\rho_1 u_1 \Delta x_1 + \cdots + \rho_n u_n \Delta x_n = \rho_f u_f \Delta x_f \tag{3.16}$$

Here the subscripts n and f are the number of cells to be merged and the final values, respectively. To define the same section of the ODT line, the merged cell size must follow $\Delta x_f = \Delta x_1 + \cdots + \Delta x_n$. For other conserved properties, Θ (i.e. species, enthalpy, etc.) a similar conservation law is used as follows:

$$\rho_1 \Delta x_1 u_1 \Theta_1 + \cdots + \rho_n \Delta x_n u_n \Theta_n = \rho_f \Delta x_f u_f \Theta_f. \tag{3.17}$$

After merging, the other conserved properties are calculated by rearranging Eq. 3.17 and substituting in Eq. 3.16, this becomes

$$\Theta_f = \frac{\rho_1 \Delta x_1 u_1 \Theta_1 + \cdots + \rho_n \Delta x_n u_n \Theta_n}{\rho_1 u_1 \Delta x_1 + \cdots + \rho_n u_n \Delta x_n}. \tag{3.18}$$

Then the velocity after merging is determined by defining $\Theta = u$ in Eq. 3.18. This results in the momentum flux conservation:

$$u_f = \frac{\rho_1 \Delta x_1 u_1 u_1 + \cdots + \rho_n \Delta x_n u_n u_n}{\rho_1 u_1 \Delta x_1 + \cdots + \rho_n u_n \Delta x_n}. \tag{3.19}$$

The resulting density is then easily calculated by rearranging Eq. 3.16, as follows:

$$\rho_f = \frac{\rho_1 \Delta x_1 u_1 + \cdots + \rho_n \Delta x_n u_n}{u_f \Delta x_f}. \tag{3.20}$$

3.2.3 Evolution Procedure

The diffusive-reactive advancement happens concurrently with the eddy events, but this section does not include the procedure for eddy events. The set of ordinary differential equations (ODEs) for both formulations are solved in time or space, using an explicit method. The first order

Euler method is described here, but a second order method is also included in the ODT code. Here the procedure is shown in terms of the temporal formulation, but the solution procedure is the same for the spatial formulation (except that the evolution variable and ODEs are different). The algorithm for ODT evolution is as follows:

1. Initialize velocity, enthalpy, and species profiles.
2. Compute mass, heat, and momentum fluxes, along with reaction source terms.
3. Then, advance the momentum, species, and energy equations (Eq. 3.7, 3.9, and 3.8) for each grid cell. This yields the velocity, energy, and species profiles after a single time step.
4. Calculate the auxiliary variables (such as temperature, mixture fraction, mixture molecular weight, etc.) from the evolving variables at the new time.
5. Update the density profile by using the ideal gas law.
6. Use the continuity equation, $\rho \Delta x = c$, to update the grid size, Δx, for all the grid cells.
7. Steps 2-6 are then repeated until the diffusion is completed.

3.3 Mesh Adaption

ODT employs an adaptive grid where more cells are placed in the location of higher gradients in a specified property (usually velocity or temperature). This is implemented by placing cells along the ODT line which have uniform arc lengths in the profile of the adapted property. To conceptually illustrate this think of a string which follows the profile of the adapted property, p(x) (where x is the ODT line direction). The string is then stretched out straight and uniform marks are made on the string. The number of cells along the string are determined by a grid density parameter, which is the number of points per unit arc length. After marking, the string is again placed along p(x), and the marks in the string indicate where in the x domain the new cell faces will be located. These new grid cells are then checked to see if they meet three constraints: they must be smaller than a given maximum size (which is almost never an issue), be larger than a prespecified minimum size, and should not be larger or smaller than its two neighbors by more than a factor of

2.5 (termed the 2.5 rule). If the cells do not fit these constraints they are either split or merged. During simulation the grid is adapted after diffusion and after eddy events occur.

3.4 Validation of Spatial ODT Code

To ensure reliability of the spatial ODT code in capturing flame structures of relevant fires, a validation of a simple flow with available experimental data was needed. An isothermal, heated wall was simulated for this purpose and compared to experiments performed by Tsuji and Nagano [59]. The isothermal wall was at a temperature of 333 K and the surrounding air was at 289 K. Figure 3.2 shows the comparison of temperature and velocity mean and root mean square fluctuation (RMS) profiles at various heights along a vertical wall. In the figure, σ is RMS fluctuations, u is streamwise velocity, and the subscripts w and ∞ denote the wall and surroundings, respectively. The temperature and velocity have been scaled in the same way as the experimental data, where δ_T and δ_m are the temperature and momentum boundary layer thicknesses, respectively. The boundary layer thicknesses were calculated using:

$$\delta_T = \int_0^L \frac{T - T_w}{T_w - T_\infty} dx, \tag{3.21}$$

and

$$\delta_m = \int_0^L \frac{u(x)}{u_{max}} dx. \tag{3.22}$$

Here T is temperature, L is the domain length, and x is distance from the wall, The mean velocity and temperature profiles have good agreement with experimental data. The experimental wall was 4 m high, but the height at which the experimental data was taken was not reported. The scaled profiles indicate that there is a similarity in the flow. ODT captures this similarity, as the profiles are very similar at the varying wall heights. The RMS velocity is underpredicted near the wall, but shows reasonable agreement with the experiment. The RMS temperature profile is overpredicted. ODT sometimes struggles to capture RMS fluctuations because it cannot capture the coherent structure of the eddies, but the simulation captures the major trends for both velocity and temperature RMS profiles. This demonstrates the ability of ODT to capture key features of a

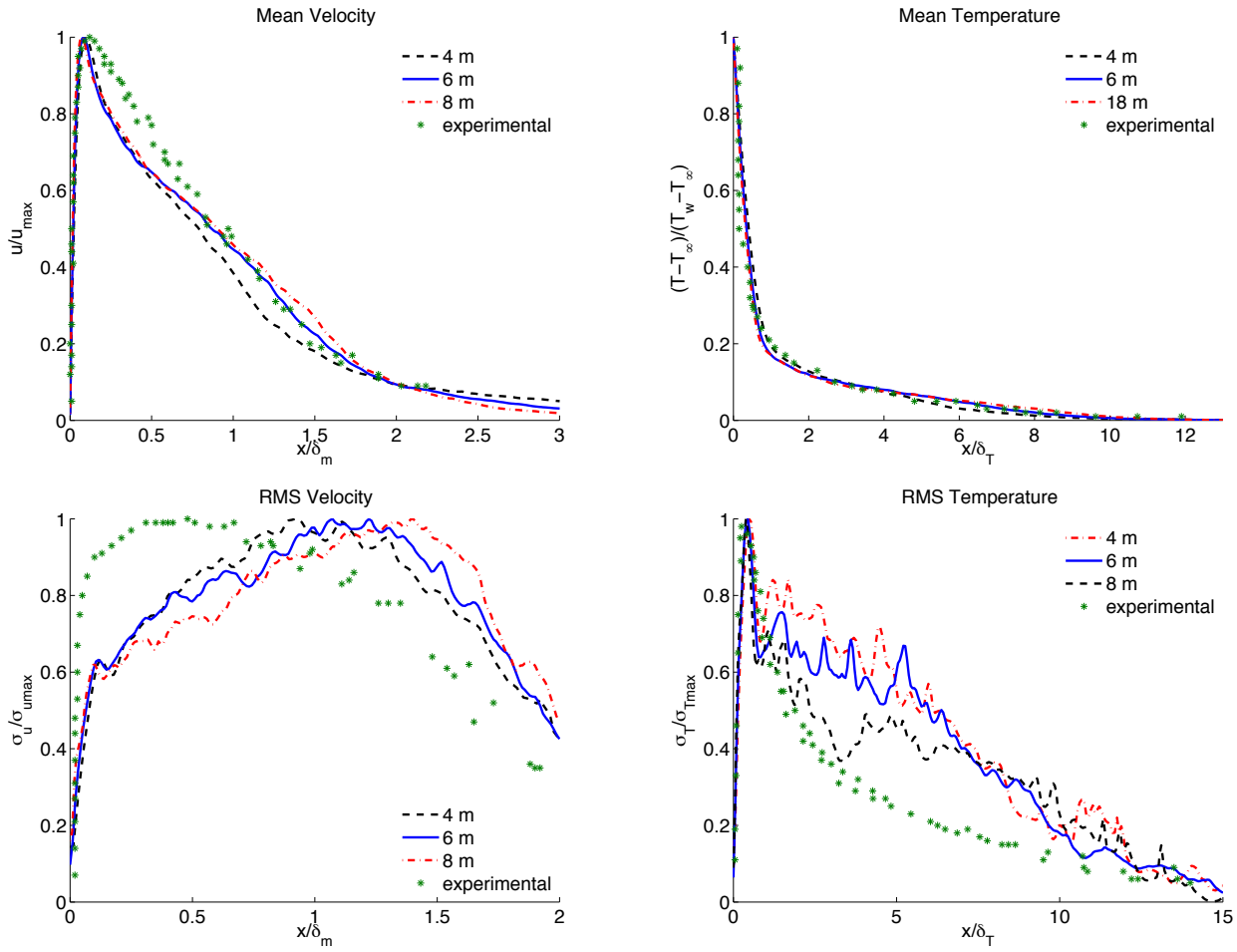

Figure 3.2: Isothermal wall mean and RMS velocity and temperature profiles at given heights. These are scaled and compared to experimental data [59].

configuration functionally similar to the flame wall configuration being investigated. For this case the ODT turbulence parameters used were C=3, Z=900, and β=1.

These results can also be compared to the work previously performed by Desjardin et al. [39], where simulations of an isothermal, heated wall were also done using ODT. Unlike the validation case in this thesis, a mean streamwise velocity was used to advance the line (which does not retain the local turbulent flows). Here, the line is advanced based on the local velocity and no averaging method is employed.

3.5 Chemical Models

Combustion chemistry consists of hundreds of chemical species and reactions, and the ODT code is capable of implementing any level of combustion mechanism complexity. Computational efficiency is determined largely through the level of complexity of the mechanism, so often simplified chemistry is used for solution.

3.5.1 One-Step and Reduced Chemical Mechanisms

Transport equations for chemical species were given (Equations 3.8 and 3.14). The chemical mechanisms are implemented through the specification of the chemical source terms found in these transport equations. These changes, however, require only a modification in the mechanism input file. The chemical source terms are implemented with Cantera [57].

The Cantera mechanism input file consists of thermodynamic information for species. A user-supplied routine is used for implementation of reaction source terms in the ODT code. Currently two mechanisms are being employed in the ODT code: (1) a global one-step mechanism for combustion of C_2H_4 with O_2 to CO_2 and H_2O products [60]; (2) a validated reduced mechanism consisting of 19 transported chemical species, 10 quasi-steady state species, and 167 chemical reactions [61]. The mechanism is based on the more complex mechanism developed by Qin [62]. This complex mechanism was written in Chemkin [63], but was reduced (by skeletal reduction) and coded into C++. The description of this reducing process is found in [61]. The transported and quasi steady state species in the reduced mechanism are: H_2, H, O, O_2, OH, H_2O, HO_2, H_2O_2, C, CH, CH_2, CH^*, CH_3, CH_4, CO, CO_2, HCO, CH_2O, CH_3O, C_2H_2, C_2H_3, C_2H_4, $C_2H_5, C_2H_6, HCCO$, CH_2CO, CH_2CHO, C_3H_6, and N_2.

The diffusive reactive system in the ODT code is computed by explicit solution of the system of ODEs presented earlier in this chapter. This requires advancement at the smallest timescale of the system to maintain numerical stability. As combustion timescales can be very small, this can result in high computational costs. The ODT code employs a method that maintains explicit solution at the diffusion time scale, but removes the stiff timescales of the chemistry by treating the local chemistry implicitly. The explicit advancement for the species is done just as with other transported variables, but with the reaction source term in the species equation replaced by its

mean rate over the step. The error in this approach is of the same order as the error in the explicit diffusion advancement. The implicit integration is performed using the CVODE software package developed at Lawrence Livermore National Laboratories [64].

3.5.2 Flamelet and Equilibrium Look-up Table Chemistry

In order to further reduce computational costs, a look-up table chemistry approach was applied to the ODT code. Another motivation for this mechanism was for its application in the solid particle implementation and to obtain acetylene concentrations when using the one-step mechanism. In this approach a conserved scalar, the mixture fraction, is used to decrease the number of scalars being transported, and thereby decrease computational costs. All the reactive species and their properties are based on this mixture fraction and the heat loss (defined as the local enthalpy defect from adiabatic normalized by the local adiabatic sensible enthalpy). The mixture fraction and enthalpy are the only two properties that are transported (rather than enthalpy and all species included in the chemical mechanism). If soot is included, soot still adds two additional transported scalars. The other properties are then linearly interpolated from preprocessed chemistry tables.

The look-up tables were preprocessed based on mixture fraction and heat loss. Two chemical methods were applied. One approach was carried out by assuming chemical equilibrium and creating an equilibrium table. Cantera [57] was used to calculate equilibrium and all properties included in the look-up table. The other approach was to generate a table using a steady laminar flamelet model [65] with a validated, reduced ethylene mechanism [61].

In the look-up table approach, it is assumed that gas reactions are fast compared to mixing and a unity Lewis number is used. The first assumption is good for this case, because combustion timescales are fast compared to mixing timescales in the flames studied and finite rate chemical kinetic effects are minor. The unity Lewis number assumption is also good, because ethylene wall fire simulations show relatively little variation between unity Lewis number and calculated diffusivities cases.

3.6 Radiation

To capture temperature profiles in fires, radiation must be modeled. Thermal radiation is emitted from both soot and gases. Soot normally accounts for the bulk of the radiation from luminous flames. Gas emission is largely from CO_2 and H_2O, with contributions from CO, and CH_4. The ODT code includes two radiation models: optically-thin and two-flux. They are described further in this section.

The first is the optically-thin model [66], which is a relatively simple model allowing for direct radiation exchange with the boundaries. There is no radiation exchange within the system. This is a good approximation when flames are small, with relatively short path length. The optically-thin model tends to overestimate radiative losses since radiation is not shielded to any degree by soot and combustion gases as radiation interacts with surroundings. This model is very simple and the radiative source term is given by:

$$q_{rad} = -4\sigma\kappa(T^4 - T_\infty^4), \tag{3.23}$$

where σ Stephan-Boltzman constant, κ is the absorption coefficient, T is the temperature, and the subscript ∞ implies the surroundings.

The two-flux model, also known as the Schuster-Schwartzchild approximation [66], is the second model employed by the ODT code. This is a common approximation in one-dimensional configurations of systems that are not optically thin. Therefore, it is a well-suited to ODT in a boundary-layer like flow.

This model assumes two radiative, oppositely-directed intensities. These intensities assume isotropic scattering in all directions on both hemispheres corresponding to the direction of the intensities. The two intensities, I^+ and I^-, are calculated along the ODT line using the following differential equations:

$$\frac{\partial I^+}{\partial x} = 2\kappa I_b - 2\kappa I^+ \tag{3.24}$$

and

$$\frac{\partial I^-}{\partial x} = -2\kappa I_b + 2\kappa I^-. \tag{3.25}$$

Here, x is the ODT line direction, κ is the absorption coefficient of the cell, and I_b is the black body intensity, $\frac{\sigma}{\pi}T^4$ (where σ is the Stefan-Boltzmann constant). The boundary conditions are defined as:

$$\frac{\partial I^+}{\partial x} = \varepsilon_0 I_{b,0} - (1-\varepsilon_0) I_0^- \tag{3.26}$$

and

$$I_L^- = \varepsilon_L I_{b,L} + (1-\varepsilon_L) I_L^+, \tag{3.27}$$

where ε_0 and ε_L are the emissivities at the left and right sides of the domain, respectively [66]. If both ε_0 and ε_L are 1, then the equations are decoupled, and may be integrated separately from the left and right sides of the domain. Otherwise an iterative approach must be taken to use this radiation model. An iterative approach was used in the ethylene wall simulations and the method is discussed in more detail in Chapter 4.

The gas absorption coefficient was calculated using a sum of species absorption coefficients weighted by partial pressure, P_i, for the gas phase:

$$\kappa_g = \sum P_i \kappa_i. \tag{3.28}$$

Here κ_i is a temperature-dependent Planck-mean absorption coefficient taken from [67]. The absorption coefficient used in Equations 3.24 and 3.25 is taken as a combination of the gas and soot values:

$$\kappa = \kappa_g + 1220 f_v T, \tag{3.29}$$

where the second term is the soot absorption coefficient with f_v the soot volume fraction. The constant 1220 on the soot absorption coefficient is related to the refractive index and is taken from [45].

3.7 Soot Model

The soot model used in the ODT code is based on a semi-empirical four-process model consisting of nucleation, growth, oxidation, and coagulation. The model is based on the work of Leung and Linstedt [68], which has been applied in many studies of turbulent sooting flames. The two moments calculated from this model are soot number density (n_s) and mass fraction (Y_s), and

their source terms are calculated using

$$S_n = \frac{2Na}{C_{min}} k_1 [C_2H_2] - 2C_a \frac{6}{\pi\rho_s}^{\frac{1}{6}} \frac{6k_bT}{\rho_s}^{\frac{1}{2}} (\rho Y_s)^{\frac{1}{6}} n_s^{\frac{11}{6}} \tag{3.30}$$

and

$$S_{Y_s} = MW_c(2k_1[C_2H_2] + 2k_2[C_2H_2]\sqrt{A_s} - k_3[O_2]A_s), \tag{3.31}$$

where Na is Avagadro's number, C_{min} is the assumed number of nucleated carbon atoms (100 in this research), k_i are reaction rate constants defined in Table 3.1, brackets indicate a concentration, k_b is the Boltzmann constant, MW_c is the molecular weight of carbon, and A_s is the soot particle surface area per unit volume. All units in these equations are SI(m, s, K, kg, mol). A_s is defied by

$$A_s = \pi \left(\frac{6\rho Y_s}{\pi\rho_s} \right)^{\frac{2}{3}} n_s^{\frac{1}{3}}. \tag{3.32}$$

The soot number density and mass fraction are dependent on the acetylene concentration, shown in Eqs. 3.30 and 3.31. The one step chemical mechanism does not include acetylene, but the other mechanisms do. If the one step mechanism is used, the acetylene concentration is found on a flamelet model look-up table. The table is based on mixture fraction and heat loss (defined as the local enthalpy defect from adiabatic normalized by the local adiabatic sensible enthalpy), which are available from the present simulation. Figure 3.3 shows the acetylene concentration as a function of mixture fraction for several values of heat loss. The stoichiometric mixture fraction is 0.063, and the acetylene, hence soot, forms on the rich side (higher mixture fractions) of the flame at mixture fractions between 0.2 and 0.25. In the figure, positive values denote heat loss, and negative values denote heat gain.

Table 3.1: Rate constants for soot reactions $k = A * e^{\frac{-E}{R*T}}$

Rate Constant ($\frac{1}{m^3*s}$)	A	E/R
k_1	$1.0E4$	21100
k_2	$6.0E3$	12100
k_3	$1.0E4$	19680

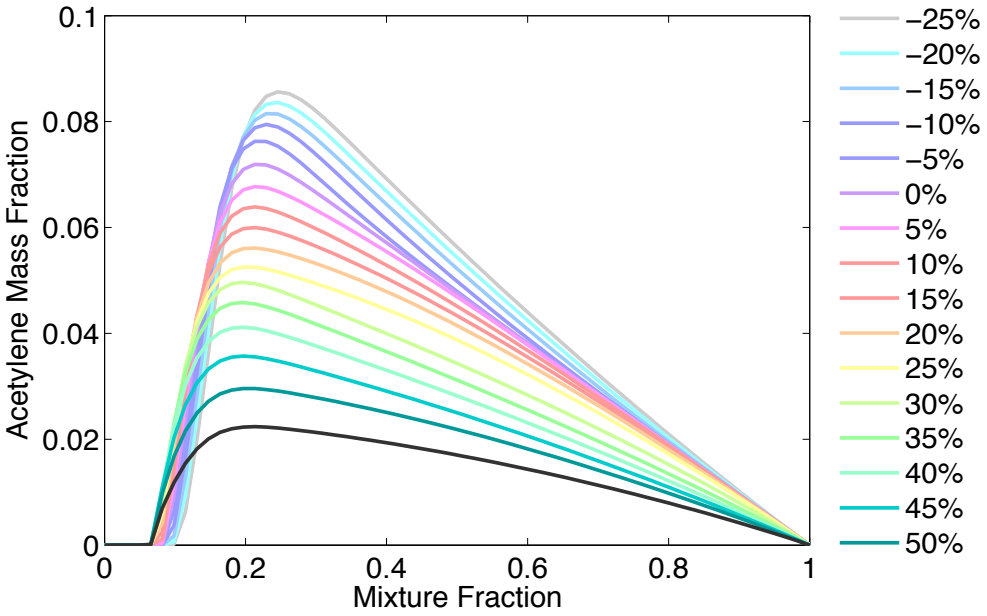

Figure 3.3: Acetylene as a function of mixture fraction for several heat losses. Positive values denote heat loss and negative values denote heat gain.

3.8 Summary

The ability to capture the intermittent and turbulent nature of a flame front is a primary interest in this research. The ODT model approximates large-scale flow and is able to resolve individual flames with realistic turbulent statistics. It is also a relatively economical turbulence modeling approach. This makes it a good option for studying these flames. The ethylene wall fire simulation carried out in this research is more amenable to a spatial formulation of the ODT. Therefore, a spatially evolving formulation was implemented into the ODT code. This spatial code was validated through simulations of an isothermal wall.

CHAPTER 4. ETHYLENE WALL FIRE SIMULATION

Due to the significance of direct flame contact to the ignition process, it is the non-steady flame front that is of primary interest in this investigation. The complexity of fires necessitates simplified fuels and configurations amenable to experimental investigation and model validation. Recent experiments have been performed on a vertical fuel source to study properties at the intermittent flame interface [5]. A vertical wall flame with ethylene fed uniformly through a porous ceramic burner approximates the behavior of a buoyantly-driven flame front inclined by gas expansion, but in a stationary configuration that eases setup, data collection and simulation.

The simulations were configured to match the experimental ethylene wall fire. The wall burner consists of an inner sintered metal layer, followed by a porous ceramic foam. The burner dimensions are 1.83 m tall, and 0.61 m wide. A fiberglass cloth borders the burner assembly in the plane of the burner. Ethylene enters through inlets on the top and bottom of the burner. Ethylene was chosen because its molecular weight is close to that of air, so that uneven flow distribution due to hydrostatic pressure was avoided. Ethylene combustion also conserves moles so that density differences are due to temperature effects. Instantaneous temperature measurements were made at four vertical stations and six horizontal positions for several fuel flow rates. Ethylene flow rates range from 115-470 standard L/min in the experiments.

Flow rates of 235, 390 and 470 L/min were studied in these simulations. Figure 4.1 shows a schematic of the configuration. The ODT domain is oriented horizontally and is perpendicular to the wall. The solution is evolved by marching upwards, described earlier in Chapter 3. Because ODT is one-dimensional, it is best suited to flows that can be approximated by boundary layer assumptions. The spatial formulation of ODT is a good model for the ethylene wall flame, because the flow is not homogeneous in the streamwise direction.

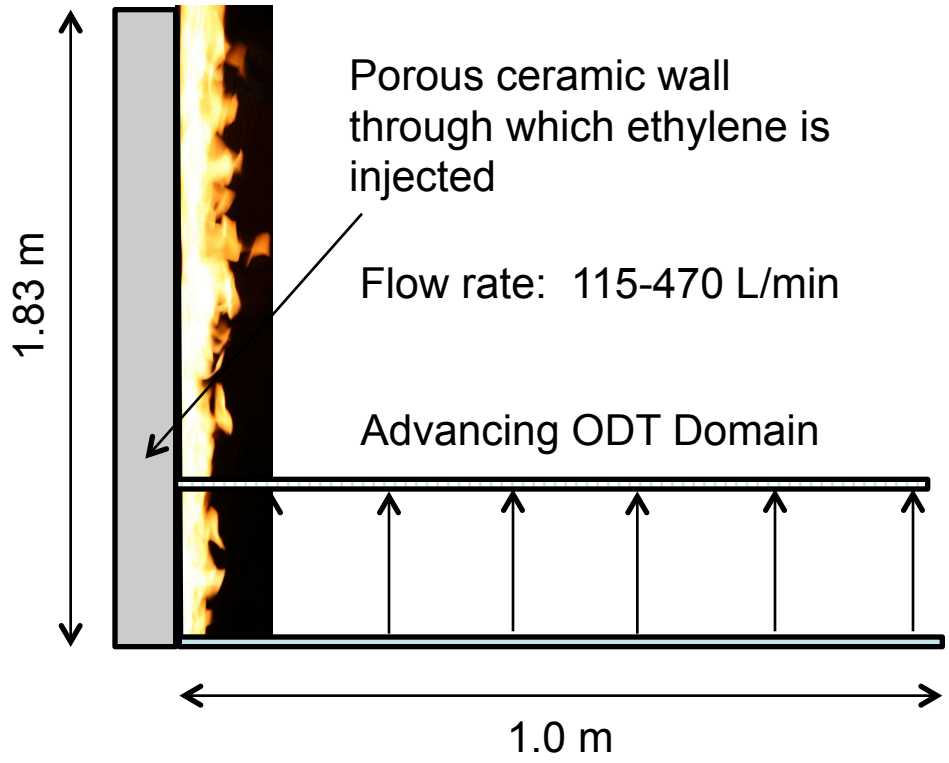

Figure 4.1: Schematic of the ethylene wall fire.

The ODT results include the velocity and temperature profiles. Mean and fluctuating temperature distributions are also given, along with probability distributions of temperature that are relevant to simulations of flame propagation in solid fuel beds.

This work represents an extension of the model in terms of the complexity of the configuration considered and is the first application of the formal spatial implementation of ODT to wall-bounded flows. Beyond this study, the successful application of ODT to buoyantly-driven, wall-bounded flows is important and would allow for detailed wall heat transfer studies.

4.1 Modeling Conditions

The key conditions that must be specified are the initial composition and velocity profiles, and the wall and outer boundary conditions for composition, velocity, temperature, and radiation. Few of these conditions are directly specified experimentally and were either modeled or inferred. The radiation and chemistry models used in this work are also discussed.

4.1.1 Initial Conditions

In the spatial ODT formulation mass flux as opposed to mass is conserved, and the transport equations are divided by velocity. The upward velocity must always be positive. Consequently, the zero-velocity boundary condition at the wall is a challenge, since the rate for all scalar transport equations diverges there. However, since there is no grid point at the wall, there is no singularity there. Here, the velocity profile is initialized as:

$$v(x) = ae^{-(\ln x - \mu_s)^2/2\alpha} + 0.1, \tag{4.1}$$

where $a = 0.5$, $\mu_s = -5$, and $\alpha = 0.75$. This gives a log-normal distribution with a small velocity magnitude. This also gives the free stream a velocity of 0.1 m/s, which is much slower than the velocities near the wall (which get up to 6 m/s). This profile was chosen due to the developed downstream velocity field being well represented by a log-normal distribution (regardless of initial profile). In the results section of this chapter the self-similar nature of the log-normal distribution is demonstrated.

The flame is initialized by specifying a mixture fraction (ξ) profile to vary smoothly (using a hyperbolic tangent transition) from unity at the wall, to zero in air. $\xi = 0$ is pure ethylene, and $\xi = 1$ is air. The transition width and its center are 5 mm from the wall. The composition profiles were then set to products of complete combustion. The temperature was calculated from the known enthalpy of the mixture, $h(\xi)$, and the composition. This initial fuel mass flux from the initial profiles is small relative to the mass flux entering the system from the wall ($<5\%$).

Figure 4.2 shows initial profiles of velocity, mixture fraction and temperature. In these figures only a portion of the domain is shown; the entire simulation domain length is 1 m. If the initial mass flux was $<10\%$ of the mass flux entering the wall, results were found to be insensitive to the free stream velocity chosen (up to 1 m/s) as well as the exact shape and location of the initial velocity and mixture fraction profiles.

4.1.2 Boundary Conditions

The wall inlet condition is implemented by inserting a new grid cell, then merging the cell with the adjacent cell if the inlet cell is small relative to the surrounding cells. However, since

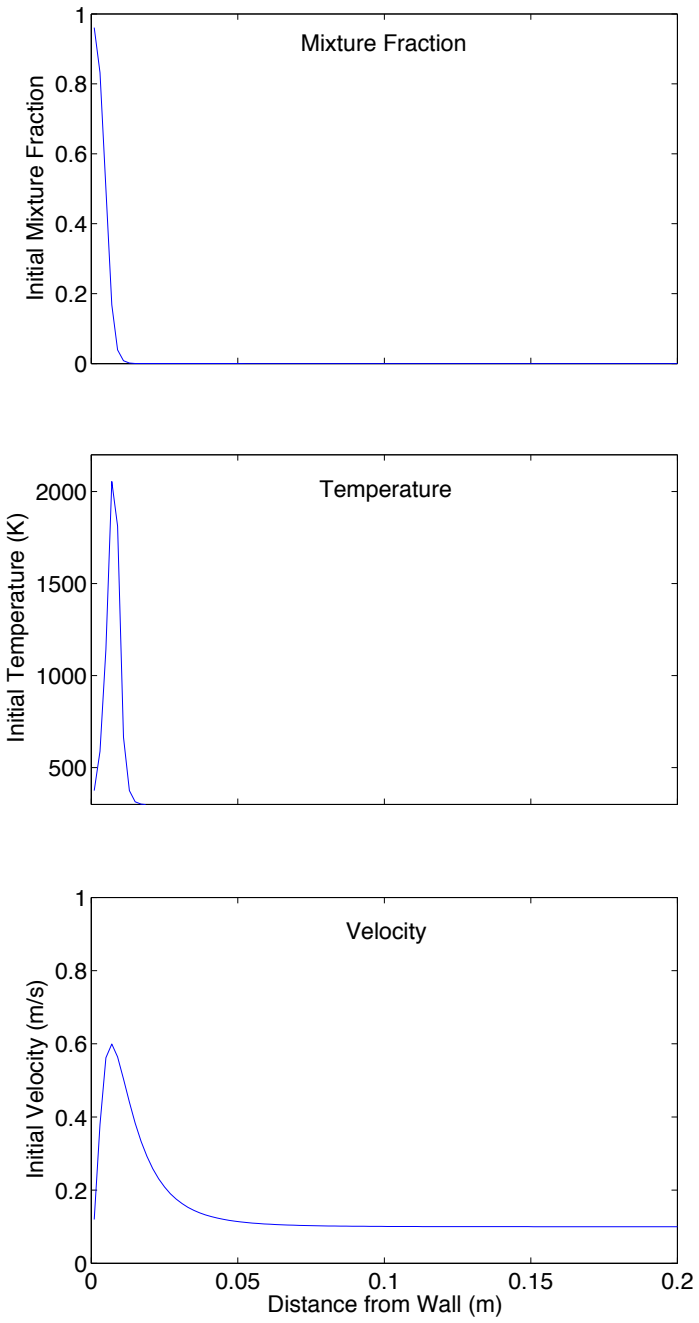

Figure 4.2: Initial profiles of mixture fraction, temperature and vertical velocity.

vertical mass flux is conserved, and there is no explicit in-line velocity component, the incoming gas is given an upward flow (zero upward velocity is prohibited in the spatial ODT formulation). The following mass flux relation is imposed: $u_{in}\Delta y = v_{in}\Delta x$, where u and x are horizontal, and v and y are vertical velocities and lengths, respectively. Mixture fraction was not included in this relation as the inlet is pure fuel. There are two degrees of freedom, v_{in} , and Δx. In this study, the v_{in} is specified by setting it equal to the velocity of the adjacent cell, hence fixing Δx. Other possible methods to specify v_{in} include linearly interpolating between the velocity in the adjacent cell and the wall (which results in a quadratic equation for v_{in}) or using the law of the wall. These are then followed by the solution for Δx. Here the temperature of the incoming fuel is 300 K.

The outer boundary condition is specified as having no gradient (no diffusive flux of mass, momentum, or energy). When the grid expands beyond the domain due to flame expansion, the excess is chopped off. If the grid contracts, due to buoyant acceleration, the last cell is extended to the desired domain size (implying that material entered the domain with the same state as the last cell, which is functionally air with the original free stream velocity).

4.1.3 Realization and Computational Details

Because ODT is a stochastic model, multiple realizations are required to obtain the flame statistics. In the results section, 1024 realizations were used to calculate the statistics (results were very similar with 128 realizations). Simulations were performed at the Fulton Super Computing Laboratory at Brigham Young University. Each simulation of 1024 realizations requires approximately 100 CPU-hours on 2.8 GHz Intel Nehalem processors. The following single set of ODT parameters were used in all simulations: C=8, Z=1000, and β=0.7.

4.1.4 Chemistry and Radiation

The results presented in this chapter are based on the one-step mechanism [60] that was discussed in Chapter 3. This mechanism is able to capture overall flame heat release. This was determined by comparing the results of the one-step mechanism to those of the reduced mechanism (discussed in Chapter 3). Figure 4.3 shows there is little difference in temperature profiles at the top of the wall between the one-step and reduced mechanism. Other properties also show little

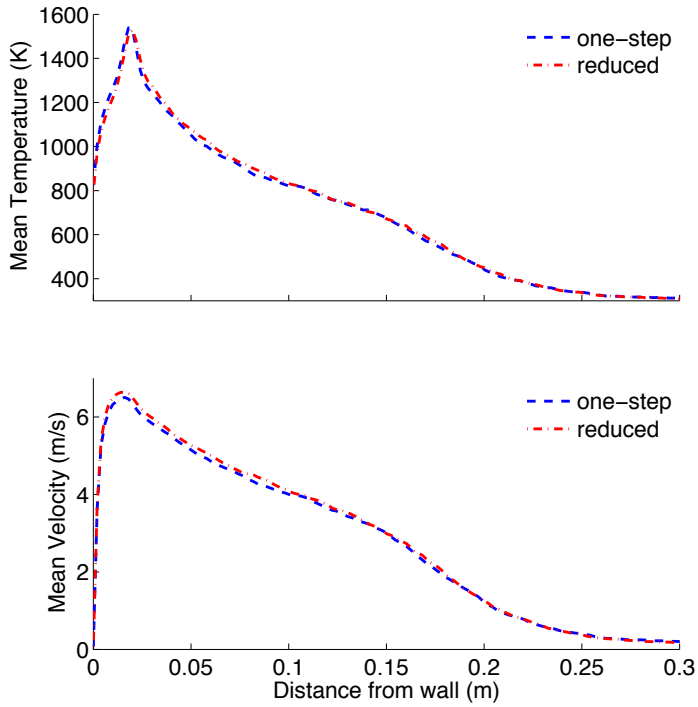

Figure 4.3: Comparison of mean temperature and velocity profiles for two chemical mechanisms.

variation when run with the reduced mechanism. This demonstrates that there is little difference in results when a more detailed chemical mechanism is applied. Therefore, to reduce computational cost, the one-step mechanism was used for these simulations.

The appropriate radiation model to use for the ethylene wall fire was determined by doing a study on the absorption coefficient at a height of 1.8 m up the wall. The predicted adsorption coefficient was used to calculate the optical thickness (τ_o) of the wall fire. When $\tau_o << 1$ the system is optically thin; when $\tau_o >> 1$ the flames are optically thick. The adsorption coefficient was plotted at a height of 1.8 m up the wall versus position from the wall for two cases: (1) with soot and radiation, and (2) with a unity Lewis number and no heat flux at the wall. These plots are shown in Figure 4.4. The non-dimensional τ was calculated from:

$$\tau_o = \int k_{abs} dx. \tag{4.2}$$

τ_o was found to be 0.44 for the sooting case and 0.32 for the adiabatic case. Therefore, the flames are neither optically thin nor optically thick. This implies that an optically thin radiation model

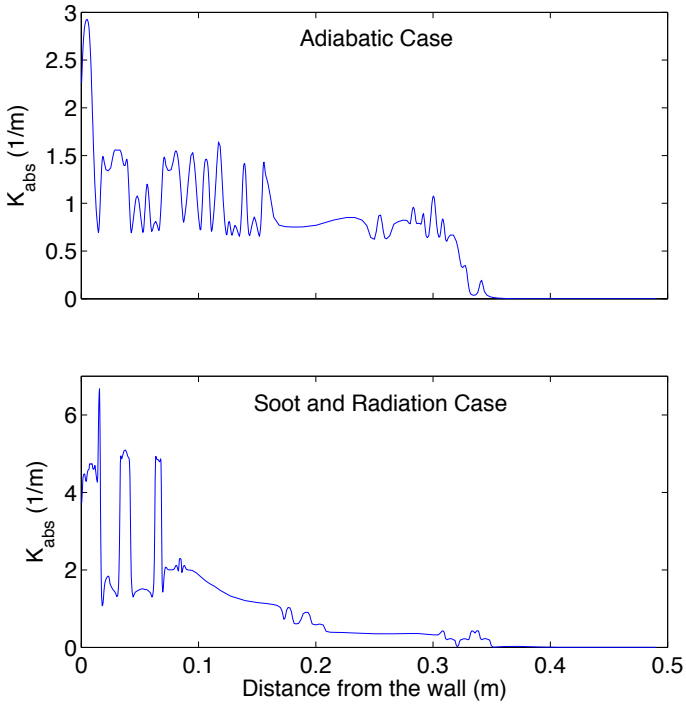

Figure 4.4: Absorption coefficient for an adiabatic case and a soot and radiation case.

would overestimate heat losses. It should be noted that this optical thickness study was done before turbulence parameters and initial conditions were optimized for the ethylene wall fire, hence different conditions were used than those reported above. The velocity was initialized with a laminar boundary layer profile rather than a log-normal distribution. The mixture fraction was initialized in the same manner as reported. The turbulence parameters were $Z = 600$, $C = 5$, and $\beta = 0.9$.

Since the ethylene wall fire isn't optically thin, the two-flux model [66] (described in further detail in Chapter 3) is used in these simulations. This is a common radiation model in one-dimensional configurations of systems that are not optically thin. Therefore, it is a well-suited to ODT in a boundary-layer like flow. To use this model, the emissivities of the boundaries must be specified. The wall emissivity is set to 1 since it is covered with a black soot. The surrounding emissivity is unknown, but is set to 0.3 since the experimental facility consists of metal walls [69].

In order to accommodate the non-unity boundary emissivity using the two-flux model in the ethylene wall fire case, a shooting method was developed. The approach was to guess a black wall and integrate I^+, followed by I^-, which then yielded the updated boundary condition for I^+.

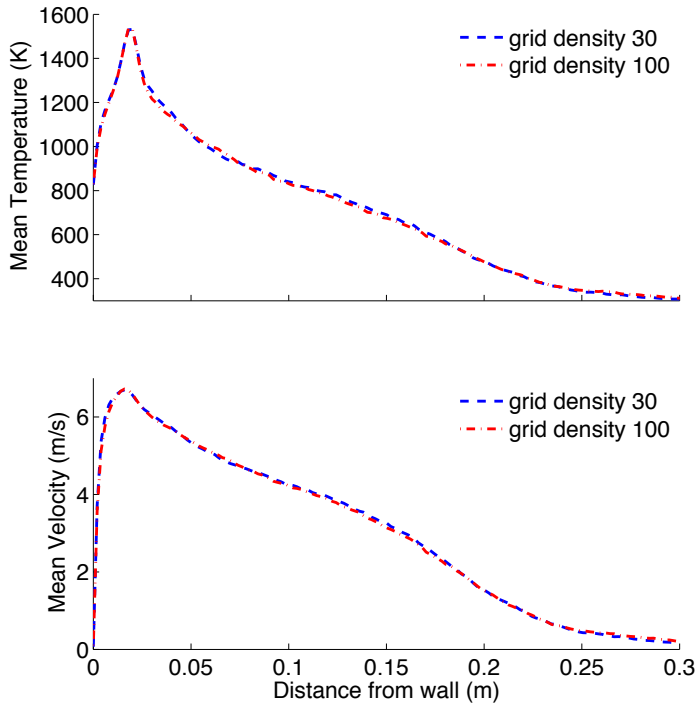

Figure 4.5: Comparison of mean temperature and velocity profiles for two grid densities.

The procedure is then repeated to convergence. Here, the wall and surrounding temperatures are assumed to be known (or known as part of the boundary condition implementation at a given point of solution).

4.1.5 Grid Resolution

One of the features of ODT is the resolution of the important physics present in the turbulent flow. In order to ensure that the ethylene wall simulations capture all the relevant scales a grid resolution study was performed. Because the grid is adaptive (the grid is already more refined where there are larger gradients), a grid density parameter is used to specify the number of grid points across the line. This parameter is discussed in Chapter 3. The ethylene wall simulations were performed with two grid density parameter values: 30 and 100 (grid cells per unit arch length). The temperature and velocity profiles at the top of the wall, for both cases, are shown in Figure 4.5. These profiles are almost identical for the two cases, which indicates that the turbulence is well resolved in both cases. This allows the use of less dense grid (using a grid density parameter of 30 rather than 100).

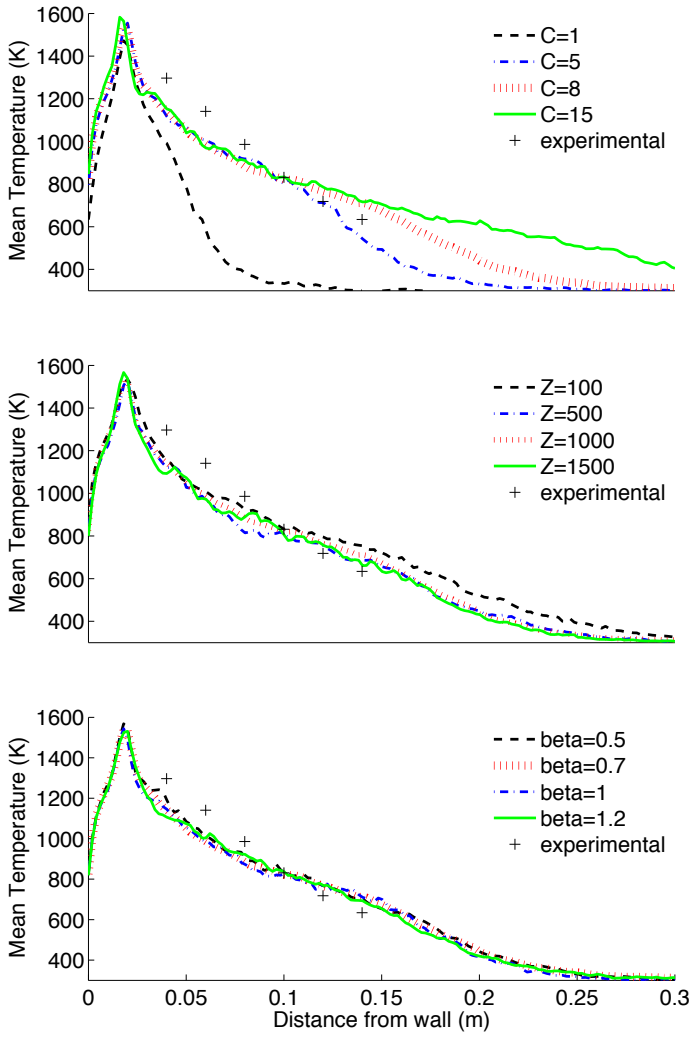

Figure 4.6: Predicted mean temperature profiles for varying model parameters (C,Z, and β).

4.1.6 Parameter Sensitivity

The ODT model uses three tuning parameters: C, Z, and β. These parameters determine the acceptance frequency and viscous penalties associated with the eddy events. A study was completed to determine the importance of each model parameter by running the ethylene wall simulations with four values for each parameter. The mean temperatures were then compared to each other and experimental data. These are shown for each parameter in Figure 4.6. These profiles indicate that the C parameter is the most significant in the ethylene wall case, while Z and β only have a small effect.

4.2 Results

The ethylene fire simulations augment data provided by experiments. These results include velocity, temperature, composition, and eddy profiles. There are four areas in which the results are presented: instantaneous (or single realization), mean and root mean square fluctuations (RMS), comparison to experimental data, and other temperature statistics.

4.2.1 Instantaneous Results

Figure 4.7 shows contours of temperature for a single typical realization. The effect of triplet maps is shown as intermittency in the flame. Buoyancy causes an upward acceleration of the flow, which draws in surrounding air. This is observed by the contraction of the flame, which is imposed by the conservation of upward mass flux in the code. Buoyant acceleration tends to cause contraction of the flow, and is opposed by flame dilatation from heat release which expands the flow. The occurrence of eddy events spreads the flame outward from the wall. While the mean profiles will be concentrated relatively close to the wall, it is clear that intermittent flame zones are present further from the wall. Figure 4.7 also shows the size and location of eddies for this particular realization. Small eddies occur close to the wall where the velocity is low but the shear is high. There is a region in the flame zone near the wall where eddies are relatively sparse, which is coincident with the highest velocities. Fewer eddies occur here because there is less shear where the velocity passes through a maximum, and the high velocity results in a reduced residence for flow in this region. It is noted that much of the turbulent mixing occurs outside the flame zone where luminous soot is not present.

A temperature profile for a given realization is shown in Figure 4.8 at a height of 1.8 m and highlights the intermittency of the flame. The plot is shown with symbols indicating the grid spacing. The adaptive grid places many more points in regions of fluctuating temperature than in regions of low temperature fluctuation, as is clear from the few points far from the wall at the right of the figure. The grid is also adapted to have a higher point density at the location of high velocity gradients, so there may be a high point density where there are small temperature gradients. This can be seen in the figure at a distance of 0.2 m from the wall. While not shown in the figure for clarity, temperature fluctuations spread with height up the wall.

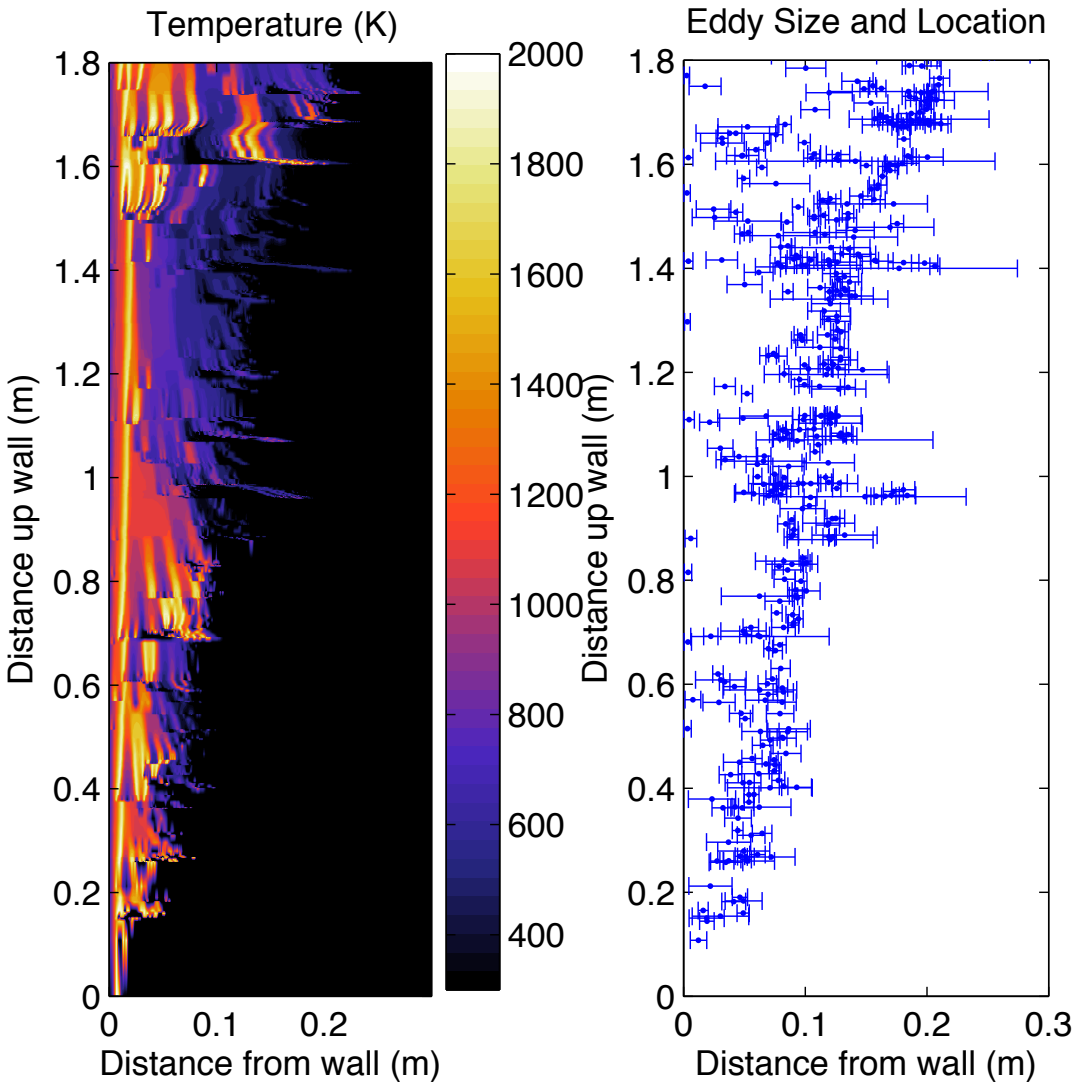

Figure 4.7: Temperature, and eddy size and location profiles for a single ODT realization.

4.2.2 Mean and Root Mean Square Profiles

Mean and root mean square (RMS) fluctuations of mixture fraction and temperature are shown in Figure 4.9 as contour plots for the 390 L/min case. The mean mixture fraction profile is shown with a contour line of the mean stoichiometric mixture fraction, $\xi = 0.064$. The mixture fraction profile widens with height due to diffusion and turbulent mixing. Due to the relatively low inlet fuel velocity entering the system, the mean stoichiometric mixture fraction remains relatively close to the wall, within 4 cm. Significant fluctuations exist at distances up to 10 cm from the wall.

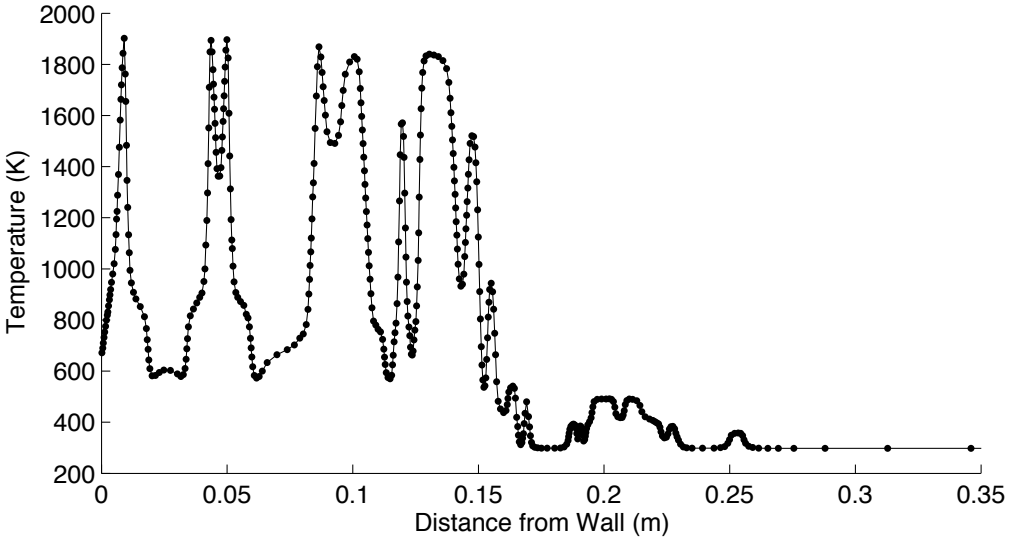

Figure 4.8: ODT temperature profile at 1.8 m of a single realization.

Mixture fraction fluctuations are highest near the wall, where the fuel is concentrated, while values are reduced towards the ambient stream away from the wall. The maximum mean temperature ($\approx$1600 K) occurs near the location of the mean stoichiometric mixture fraction. Mean temperatures as high as 800 K reach 10 cm from the wall, consistent with the mixture fraction fluctuations. While the peak temperature remains relatively close to the wall, the temperature profile is observed to spread significantly. This is mirrored by the RMS profiles, with higher values penetrating further into the free stream. The peak RMS temperature occurs near the base of the wall as the turbulent eddies first wrinkle the initial flame.

Mean velocity profiles at 0.2, 1.0, and 1.8 m up the wall are shown in Figure 4.10 for the 390 L/min flow rate. Buoyancy causes the velocity to accelerate up the wall, and the maximum mean velocity reaches approximately 6.5 m/s. The velocity profiles increase in magnitude and width with downstream distance. The profiles have the same shape and are very nearly similar when scaled by the max velocity and the width of the profile at half the maximum velocity, especially for profiles at heights above 0.5 m. This similarity is consistent with previous reports [56, 70], and motivates the use of the initial velocity profile noted above.

The mean soot field, shown in Figure 4.11 is limited to the rich side of the flame, close to the wall, and concentrated in regions within 2 cm, though fluctuations cause soot to appear further

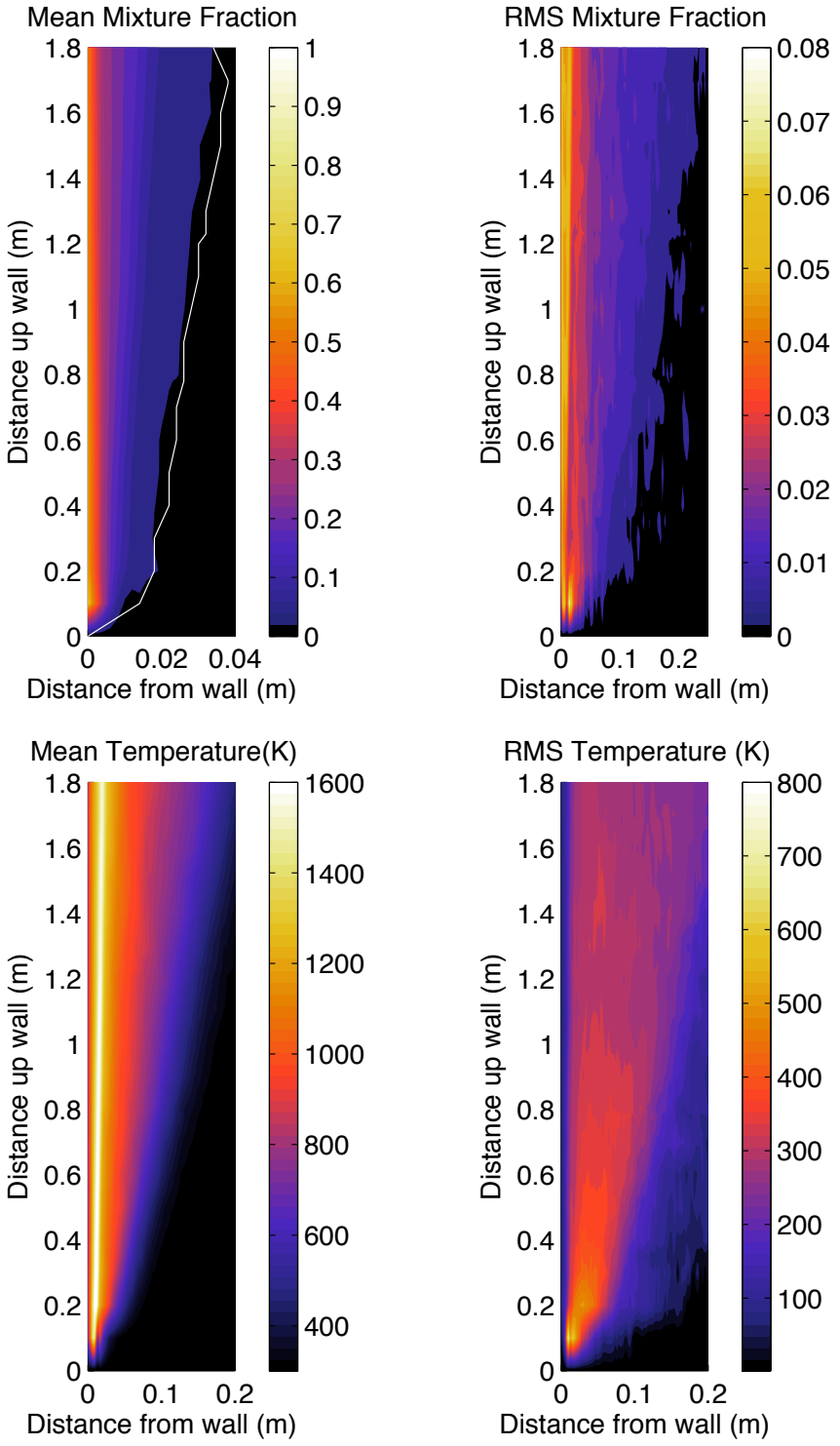

Figure 4.9: Mean and RMS mixture fraction and temperature for fuel flow rate 390 L/min. The stoichiometric mixture fraction contour is shown.

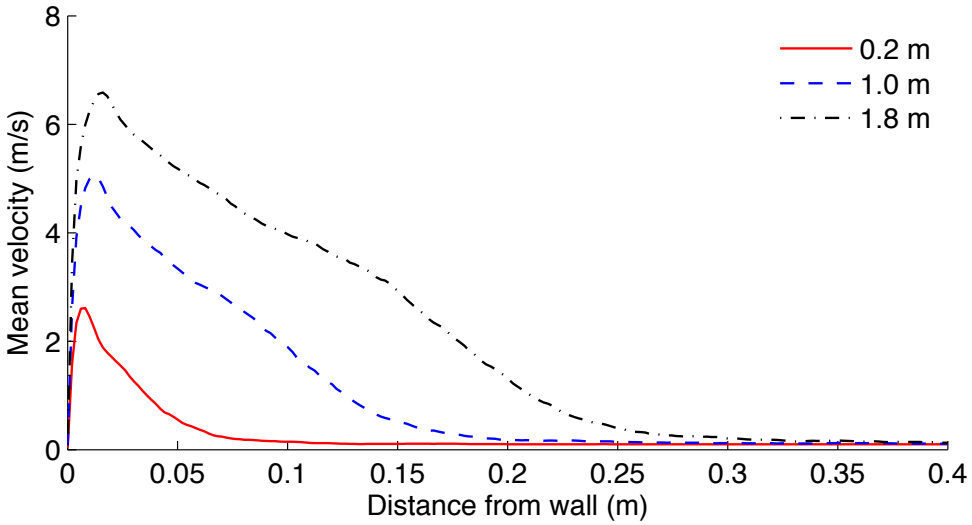

Figure 4.10: Mean velocity profiles at three heights at 390 L/min.

from the wall. The mean soot concentration is approximately 4 ppmv and is fairly uniform in the fuel side of the flame due to turbulent mixing. However, the soot concentration is high at the base of the wall (because of higher formation rates), but the soot then mixes and/or reacts to become more uniform as it advances up the wall.

4.2.3 Comparison to Experimental Data

Mean temperature profiles for three fuel flow rates of 235, 390, and 470 L/min are shown in Figure 4.12. The figure compares the ODT simulation results to experimental measurements. The experiments were performed by Finney et al. [5]. The temperature measurements were made at heights of 0.35, 0.78, 1.23, and 1.69 m. At the first height, an array of six thermocouples were placed at distances of 3, 5, 7, 9, 11, and 13 cm from the wall; at the other three heights six thermocouples were placed at 4, 6, 8, 10, 12, and 14 cm from the wall. The figure shows four plots at each height, with three flow rates on each plot. Simulation results are shown as solid lines and experimental measurements as symbols.

At a given height, peak temperatures are similar for the three flow rates studied, while the location of the peak increases from the wall with increasing flow rate. These distances of peak temperature are shown in Table 4.1. Similarly, the temperature on the air side of the peak, in the

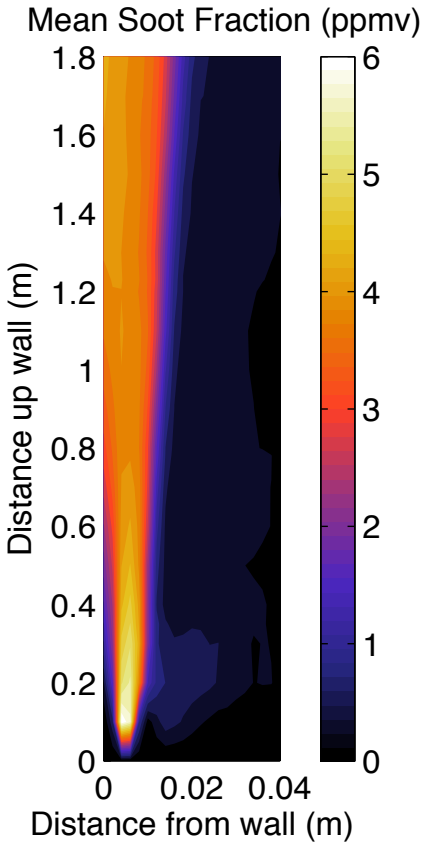

Figure 4.11: Mean soot profile at 390 L/min.

Table 4.1: Maximum mean temperatures and locations at height of 1.8 m for three flow rates.

Ethylene Flow Rate (L/min)	Maximum Mean Temperature (K)	Location from wall (cm)
235	1540	1.4
390	1550	1.8
470	1550	2.0

measurement region, increases with increasing flow rate as the width of the flame brush increases with increasing flow rate, evidenced by the longer temperature tail at higher fuel flows. For a given flow rate, the peak temperature decreases with increasing height, as radiative transport reduces flame temperatures. In contrast to temperature, the peak velocity increases with increasing flow rate, while the location of the peak from the wall remains similar. This is quantified in Table 4.2.

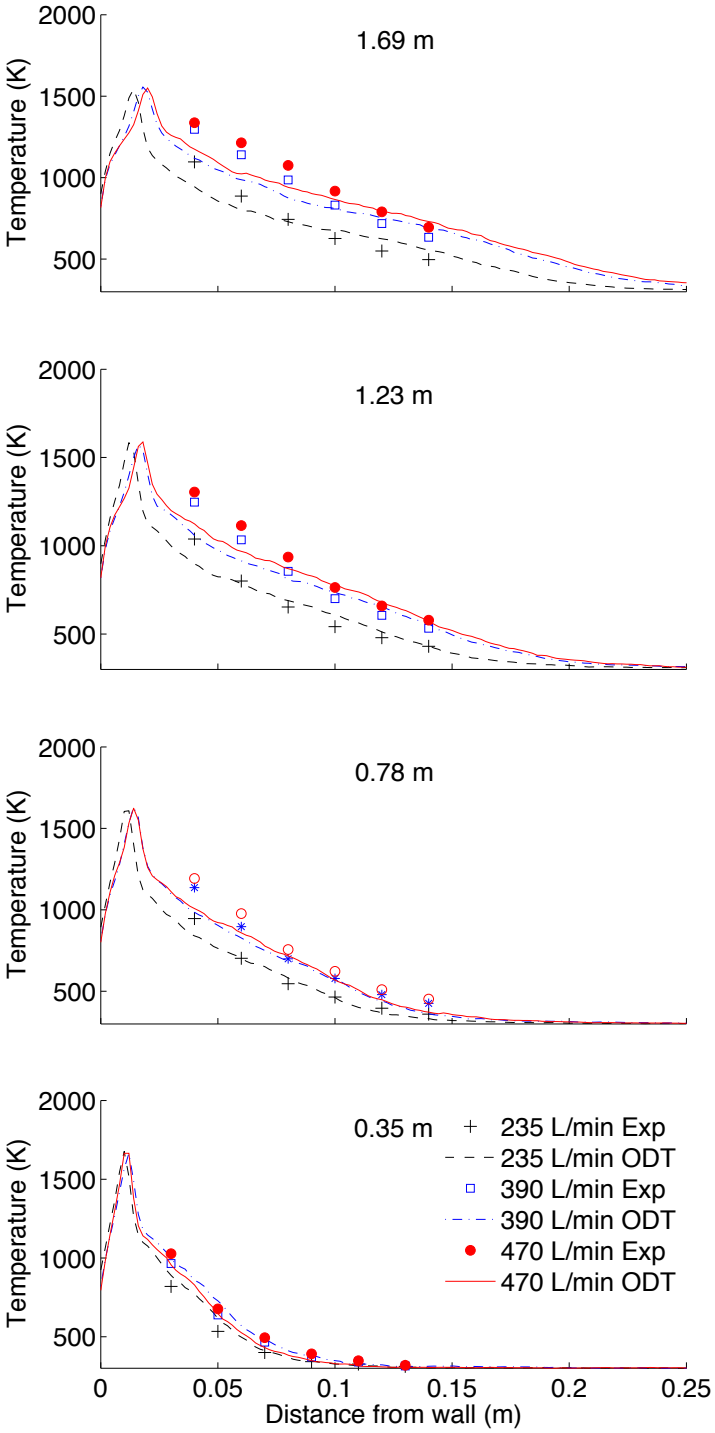

Figure 4.12: Experimental and ODT mean temperatures at four heights for three flow rates.

Table 4.2: Maximum mean velocities and location at height of 1.8 m for three flow rates.

Ethylene Flow Rate (L/min)	Maximum Mean Velocity (m/s)	Location from wall (cm)
235	6.0	1.63
390	6.4	1.65
470	6.5	1.65

The ODT comparison to the experiments is good. At a given height and horizontal distance, the spread in the data with flow rate is closely matched by the spread in ODT results. Agreement is best at the lowest wall height. At the upper measurement station, simulated temperatures are as much as 15% lower than the measurements in the region nearest the peak flame temperature.

It was first assumed that this temperature difference near the upper measurement station was due to the fact that the experimental temperature measurements were not corrected for radiation. Therefore, a simulation was performed, where predicted radiation effects were applied to the experimental thermocouples. This was done by applying the following energy balance to the thermocouples

$$h_0(T_{corrected} - T_{thermocouple}) = \varepsilon\sigma T_{thermocouple}^4 - \pi(I^+ + I^-), \tag{4.3}$$

where T is temperature, h is the heat transfer coefficient, ε is the thermocouple emissivity, and I^+ and I^- are the two local, radiative intensities of the two-flux radiation model defined in Chapter 3. Since the thermocouples were covered in a thin soot layer, ε was assumed to be one. The heat transfer coefficient was calculated from the Nusselt number correlation reported by Ranz and Marshall [71]:

$$Nu = 2 + 0.6Re^{\frac{1}{2}}Pr^{\frac{1}{3}}, \tag{4.4}$$

where Re and Pr are the Reynolds and Prandlt number evaluated with the thermocouple diameter (0.1 mm) and local gas phase properties. $T_{thermocouple}$ was set to be the mean experimental thermocouple temperature. Equation 4.3 was then arranged to solve for $T_{corrected}$. This was done for all the experimental thermocouple locations.

The experimental, thermocouple mean temperatures are compared to the corrected values in Figure 4.13. The correction has little effect on the mean temperatures nearest the wall, but the thermocouple temperatures decrease as distance from the wall increases. Also, these effects are greater at the base of the wall and decrease with height. Therefore, the fact that the thermocouples were not being corrected for radiation is not the cause of the ODT under-prediction of temperatures near the wall. Instead, this under-prediction is likely due to an over prediction of radiative heat loss (which losses are highest near the flame), which is consistent with our use of Plank mean gas absorption coefficients, the two-flux model, and the inherent uncertainties in all soot models. It is noted that results in the measurement region are on the lean side of the flame (lean in the mean) where soot concentrations are very low, so that depressed temperatures are due to a combination of radiation and mixing with ambient air. Still, the comparison is reasonable.

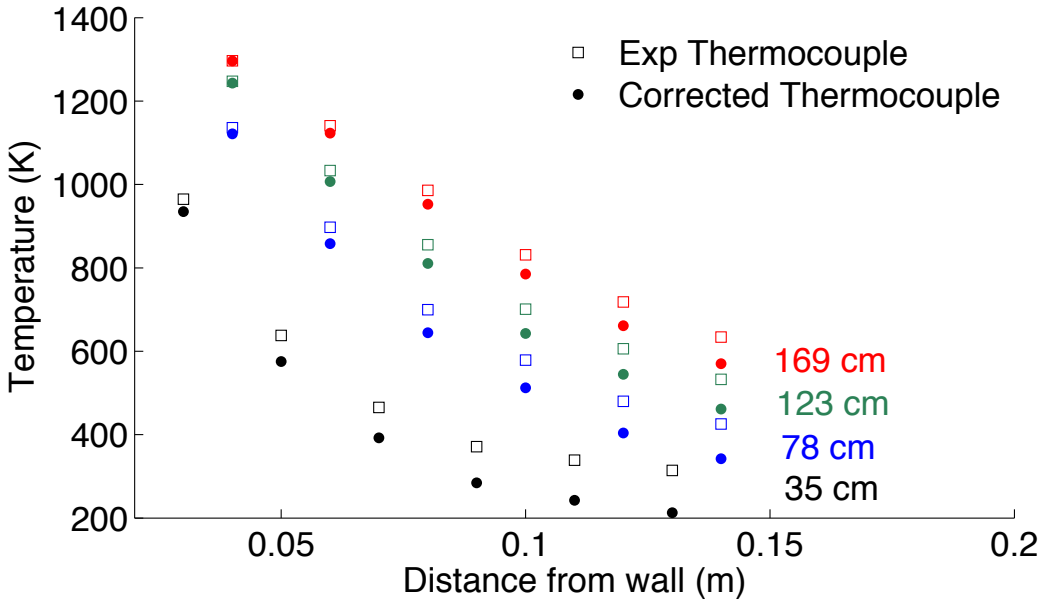

Figure 4.13: Comparison of experimental and radiation corrected thermocouple temperatures.

Figure 4.14 shows a comparison of the RMS temperature fluctuations for the 390 L/min case to the experimental fluctuations. The data show a decrease in temperature fluctuation with distance from the wall at the lowest height. At the other three heights, the fluctuations show a mild peak with distance. The ODT model results over predict the RMS fluctuations. The decreasing

trend is generally observed, however, with a similar slope as the data. A peak in the ODT fluctuation profile is only clearly visible at the 78 cm height. Capture of RMS fluctuations can be difficult in ODT, which lacks the ability to capture multi-dimensional turbulent structures. ODT simulation of channel flow generally under predicts velocity fluctuations by around 33% (compared to DNS results) due to the inability to capture sweeping structures. ODT comparisons of temperature RMS are similar in DNS of flame extinction and reignition of temporally-evolving jets prior to flame extinction. It is noted that experimental results were obtained using type-K thermocouples whose upper range (around 1500 K) is not high enough to capture individual flamelets. The time-dependent experimental data did not have any temperatures higher than 1600 K, while the model predicted intermittent temperatures as high as 2000 K. If higher experimental peak temperatures were reached, then the experimental RMS fluctuations would be higher. RMS fluctuations for the other flow rates are not shown because they have similar trends and comparisons.

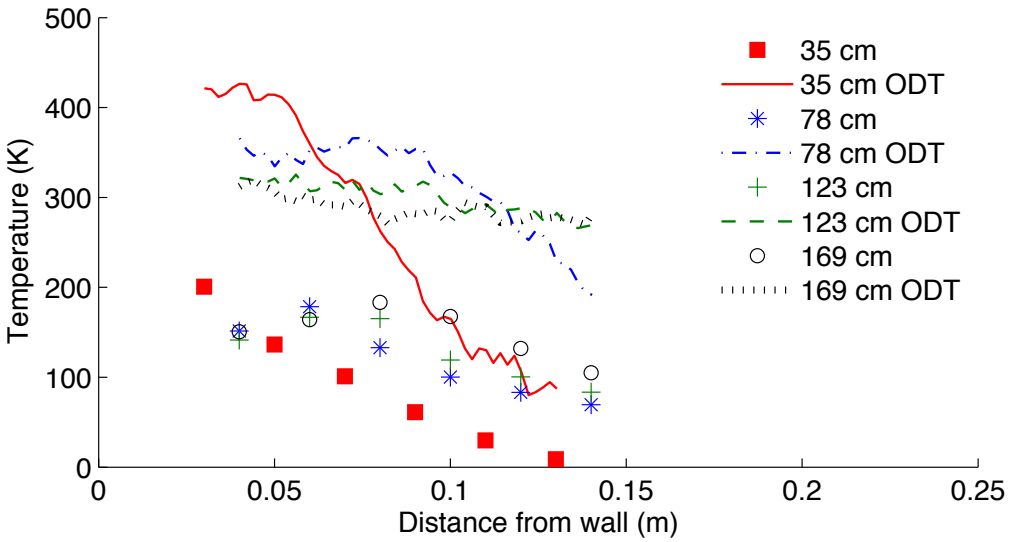

Figure 4.14: Comparison of experimental and ODT RMS temperatures at four heights at 390 L/min.

4.2.4 Other Temperature Statistics

ODT simulation provides a wealth of statistical data that is useful for investigation of fluctuating temperature fields. These data are important in the study of flame propagation.

Figure 4.15 shows the power spectral density of temperature (PSD) in the time domain for the ethylene fire at two distances from the wall at a height of 1.8 m. Here the PSD are plotted versus frequency (f) rather than wave number, to indicate the important frequencies. These PSDs have an inertial region where the power spectral density is proportional to $f^{-5/3}$, which is expected in turbulent flow [12]. Most of the energy is found in the region with lower frequencies than those in the inertial region. The temperature fluctuations in the inertial region or with even higher frequencies are not significant. The important frequencies decrease with distance from the wall.

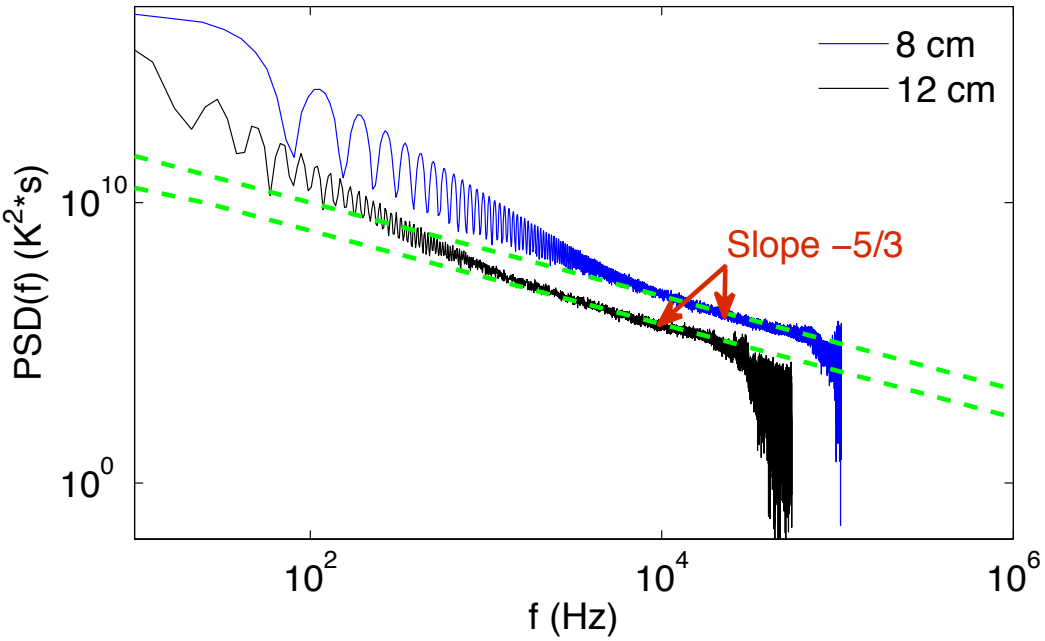

Figure 4.15: PSD of temperature at the top of the wall at two distances from the wall.

Probability distributions of temperature are of particular interest. These distributions of resolved temperature fields are unique to ODT. Transported probability density function methods give similar results, but rely on empirical mixing models in state space as opposed to direct mixing and transport in the physical coordinate as performed in ODT. The temperature data in ODT is being used in a follow-on study in which solid fuels are heated to ignition and burned at the interface of a turbulent flame brush. As an example, Figure 4.16 shows two plots of the probability of temperatures greater than 600 K, and 1000 K as a function of position. The probability increases

with height at a given horizontal position, indicating the flame spread. The higher temperature plot is clearly closer to the wall. These results are important for fuels with a given ignition temperature.

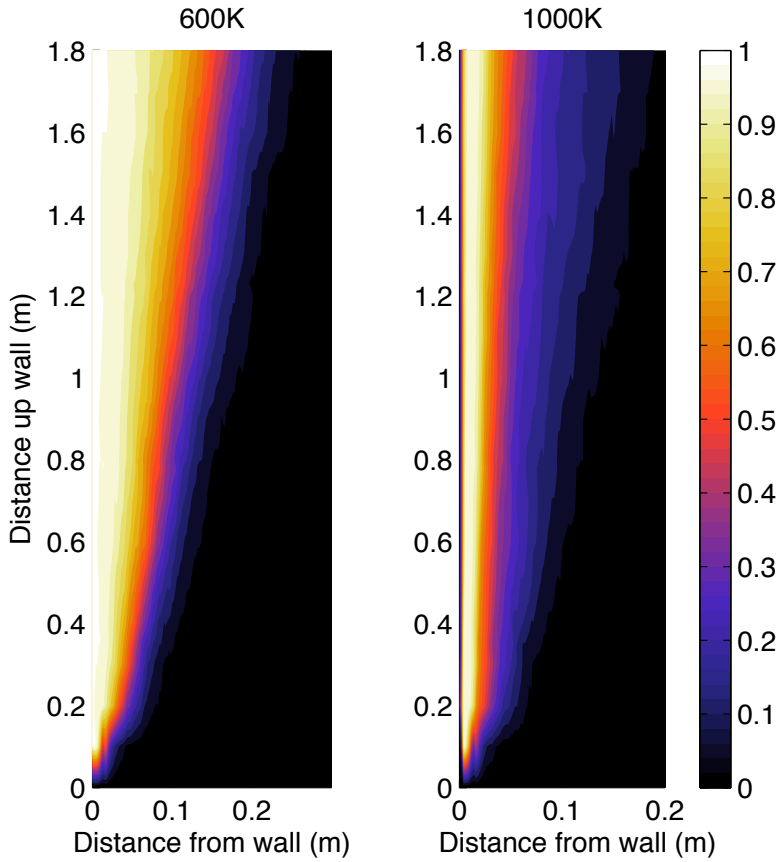

Figure 4.16: Probability of temperature greater than 600 and 1000 K at 390 L/min.

In addition, at any given spatial location, a full temperature PDF may be computed. Figure 4.17 shows PDF plots of temperature for 0.02, 0.05, 0.1, and 0.15 meters from the wall at a height of 1.8 m for the 390 L/min flow rate. Twenty-five bins are used in these PDFs (with 5000 ODT realizations). The horizontal locations correspond to rich, approximately stoichiometric, and lean positions relative to the mean flame location. There are two PDF locations (furthest from the wall) corresponding to the lean region, because this is the area of greatest interest. At these two positions, the profiles become bimodal, because significant amounts of ambient air are entrained.

This indicates the extent of the intermittent flame behavior at the flame front. Moving away from the wall, the peak in the PDF shifts towards lower temperatures and decreases in width.

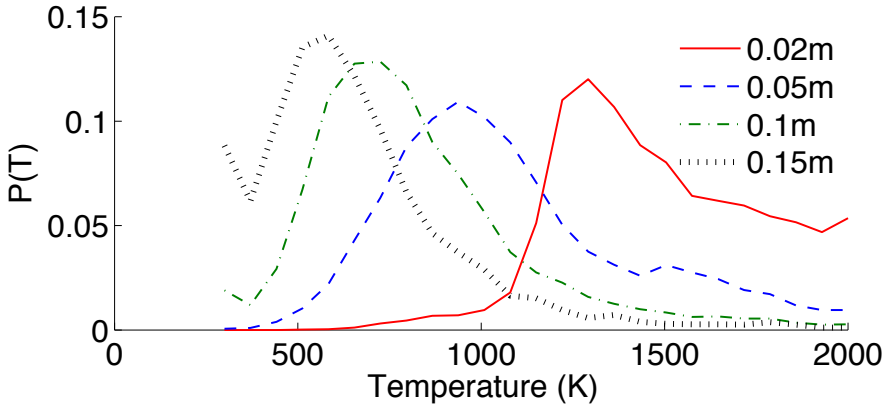

Figure 4.17: PDFs of temperature at a height of 1.8 m at four distances from the wall at 390 L/min.

4.3 Conclusions

ODT simulations have been performed of an ethylene wall flame using a modern spatial formulation. The model was compared with experimental results in which ethylene is fed at varying flow rates through a porous wall burner. The configuration was chosen to mimic the behavior of a turbulent flame brush at the interface of a nominally vertical flame front in a wildland fire propagating through a dense fuel bed. As combustion gases rise, flames become inclined due to flame dilatation. In such flows, flame spread by direct flame contact has been found to be important. The ODT model resolves diffusion-reaction flame structures in one dimension, with physically-realistic turbulent statistics arising through the advective processes in the model. This allows detailed temperature fluctuations to be modeled. ODT simulation results were presented of mean and fluctuating temperature, mixture fraction and velocity profiles. Agreement with experimental results was generally good, though predicted temperatures were up to 15% below experiments in the flame zone, and temperature fluctuations were over-predicted. PDFs of temperature were presented to illustrate model capabilities. This paper is part of a larger study to understand flame propagation in fuel beds. This work has demonstrated the application of ODT to the problem of

interest. The mean, fluctuating, and probability temperature distributions given in this study are relevant to simulations of flame propagation in solid fuel beds.

CHAPTER 5. SOLID PARTICLE COMBUSTION

In order to extend the capabilities of the ODT to the study of flame propagation in solid fuel beds representative of wildland fires, solid fuels were incorporated into the model. In this study the particles are stationary and act as the fuel source. As wood is composed of a high amount of volatiles (70-90%) [72, 73], this work focuses only on the pyrolysis of the wood. Char combustion is not included in this implementation. This work represents the first application of the ODT model to wood particle pyrolysis in a turbulent flow, and can be directly applied to the study of flame spread in a fuel bed.

Incorporation of solid fuels into the ODT requires both particle and gas phase governing equations. This chapter derives the new gas-phase equations and particle governing equations, discusses the solution procedure, and includes preliminary results.

5.1 Derivation of Lagrangian Transport Equations in the Gas Phase

As with the standard temporal and spatial formulations given in Chapter 3, the derivation for the solid particle equations also begins with the Reynolds transport theorem as the base for the derivation of the respective Lagrangian transport equations. Although these equation can evolve either temporally or spatially, this derivation covers the temporally evolving equations. The spatial formulation is similar and has also been implemented into the code. As a simple mixture fraction chemistry approach (explained in further detail in the particle chemistry section) is taken, there are no species being evolved, but rather a single mixture fraction.This method also implies that a unity Lewis number is assumed and the heat flux in the energy equation is defined differently that that in the standard temporal or spatial formulation.

The system Ω is defined as a fixed mass of fluid that can be either a mixture or a single component. Then the system boundary Π moves at the velocity of the mass defining the system,

and therefore no mass crosses the system boundary. The Reynolds transport theorem is given by

$$\frac{\partial}{\partial t}\int_{\Omega(t)} \rho\eta dV = \int_{\hat{\Omega}} \frac{\partial \rho\eta}{\partial t} dV + \int_{\hat{\Pi}} \rho\eta \vec{v}_{sys} \cdot \vec{n} dA. \tag{5.1}$$

Here η is an intensive variable (some conservation property per unit mass) to be transported, ρ is the system density, $\vec{v}_{sys}$ is the system velocity, $\Omega(t)$ is the Lagrangian system, $\hat{\Omega}$ is the Eulerian control volume corresponding to Ω at a given t, and $\hat{\Pi}$ is the boundary of $\hat{\Omega}$. If the control volume $\hat{\Omega}$ and its corresponding boundary move with the velocity $\vec{v}_{cv}$, then the Lagrangian transport equation is then

$$\frac{\partial}{\partial t}\int_{\Omega(t)} \rho\eta dV = \int_{\hat{\Omega}(t)} \rho\eta dV + \int_{\hat{\Pi}} \rho\eta \vec{v}_R \cdot \vec{n} dA, \tag{5.2}$$

where $\vec{v}_R = \vec{v}_{sys} - \vec{v}_{cv}$.

5.1.1 Mass Conservation Equation

The control volume for the mass conservation equation is defined so that is moves with the gas mass average velocity. Then let η equal 1 and the system be defined as the mass of the gas only; the particle mass is not included. With this defined control volume and system, $\vec{v}_R$ is equal to 0 and there is a mass source term from the pyrolyzing particle. Equation 5.2 then becomes

$$\frac{\partial}{\partial t}\int_{\hat{\Omega}} \rho dV = \int_{\Omega} S_\phi dV, \tag{5.3}$$

where S_ϕ is the gas fuel source term per cell volume defined in the particle equations section of this chapter. There is an addition of a void fraction (or volume fraction of gases per total cell volume), γ, when integrating over the control volume because the particles are not included in the system. This means the control volume is $\gamma * \Delta x$. The γ will vary in line position (x) and time (t), and is also explained further in the particle equations section of this chapter. After integrating Equation 5.3, the mass conservation equation is

$$\frac{\partial(\rho\gamma\Delta x)}{\partial t} = S_\phi \Delta x \gamma, \tag{5.4}$$

where Δx is the cell size. Notice that the mass is no longer a constant, but has a source term (before $\rho\Delta x$ was constant). This will create source terms in all the governing equations.

5.1.2 Momentum Equation

Again the system and control volume velocities are defined as the gas mass average velocity and equal so $\vec{v}_R = 0$. Here $\eta = \vec{v}$ (the gas phase velocity vector) and Equation 5.2 yields

$$\frac{\partial}{\partial t}\int_{\Omega(t)} \rho\vec{v}dV = \frac{\partial}{\partial t}\int_{\hat{\Omega}(t)} \rho\vec{v}dV. \tag{5.5}$$

The rate of change in momentum must equal the applied force. By substituting this definition into equation 5.5 it becomes

$$\frac{\partial}{\partial t}\int_{\Omega} \rho\vec{v}dV = \int_{\Pi} \vec{F}_{ext}dA = -\int_{\Pi}(P\delta + \tau)\cdot\vec{n}dA, \tag{5.6}$$

where $\vec{F}_{ext}$ is external force applied to the system and P is pressure. The direction of velocity u (in y) is perpendicular to the ODT line. The stress tensor is defined as $\tau_{yx} = -\mu\frac{\partial u}{\partial x}$ where μ is the local viscosity. By integrating Equation 5.7 and rearranging the equation for u is then

$$\frac{\partial(\rho u\gamma\Delta x)}{\partial t} = -\Delta x\gamma\frac{\partial P}{\partial y} - (\tau_{yx,e} - \tau_{yx,w}). \tag{5.7}$$

where e and w denote the east and west faces of the control volume. Then by applying the definition of a derivative of products to the left side of the equation and by dividing by $\rho\gamma\Delta x$ the equation becomes

$$\frac{u}{\rho\gamma\Delta x}\frac{\partial(\rho\gamma\Delta x)}{\partial t} + \frac{\partial u}{\partial t} = -\frac{\partial P}{\partial y}\frac{1}{\rho} - \frac{\tau_{yx,e} - \tau_{yx,w}}{\rho\gamma\Delta x}. \tag{5.8}$$

Substituting the mass conservation equation in the first term and rearranging the momentum equation yields

$$\frac{\partial u}{\partial t} = -\frac{\tau_{yx,e} - \tau_{yx,w}}{\rho\gamma\Delta x} - \frac{1}{\rho\gamma}\frac{\partial P}{\partial y} - \frac{uS_\phi}{\rho}. \tag{5.9}$$

5.1.3 Energy Equation

For the energy equation, η is defined as the internal energy per unit mass (e) in Equation 5.2. The system is defined similarly to the momentum equation where the system contains the gas mixture mass only so the system and control volume have the same velocities and $\vec{v}_R = 0$. The Lagrangian energy equation is then

$$\frac{\partial}{\partial t}\int_\Omega \rho e dV = \dot{Q} + \dot{W} = -\int_\Pi \vec{q}\cdot\vec{n} - \int_\Pi \vec{F}_{ext}\cdot\vec{v}_{sys} dA, \tag{5.10}$$

where Q is the heat added to the system, W is the work on the system, and q is the heat flux. Only pressure work is considered and the equation becomes

$$\frac{\partial}{\partial t}\int_\Omega \rho e dV = \dot{Q} + \dot{W} = -\int_\Pi \vec{q}\cdot\vec{n} - \int_\Pi P\vec{v}\cdot\vec{n} dA. \tag{5.11}$$

Then by substituting in the definition of internal energy, $e = h - \frac{P}{\rho}$, and integrating over the control volume this yields

$$\frac{\partial}{\partial t}(h\rho\Delta x\gamma - P\Delta x\gamma) = -(q_e - q_w) - P(\hat{u}_e - \hat{u}_w). \tag{5.12}$$

Then by applying the definition of a derivative of products to the left side of the equation and by dividing by $\rho\gamma\Delta x$ the equation becomes

$$\frac{\partial h}{\partial t} + \frac{h}{\rho\gamma\Delta x}\frac{\partial(\rho\gamma\Delta x)}{\partial t} - \frac{1}{\rho}\frac{\partial P}{\partial t} - \frac{P}{\rho\gamma\Delta x}\frac{\partial(\Delta x\gamma)}{\partial t} = -\frac{q_e - q_w}{\rho\Delta x\gamma} - \frac{P}{\rho\Delta x\gamma}(u_e - u_w). \tag{5.13}$$

Substituting the mass conservation equation into the second term and rearranging the equation is then

$$\frac{\partial h}{\partial t} = \frac{P}{\rho\Delta x\gamma}\frac{\partial(\Delta x\gamma)}{\partial t} + \frac{1}{\rho}\frac{\partial P}{\partial t} - \frac{q_e - q_w}{\rho\Delta x\gamma} - \frac{P}{\rho\Delta x\gamma}(u_e - u_w) - \frac{hS_\Phi}{\rho}. \tag{5.14}$$

The first and fourth term on the right side of Equation 5.14 are equal and therefore cancel out. Then the energy conservation equation becomes

$$\frac{\partial h}{\partial t} = \frac{1}{\rho}\frac{\partial P}{\partial t} - \frac{q_e - q_w}{\rho\Delta x\gamma} - \frac{hS_\Phi}{\rho}. \tag{5.15}$$

The heat flux, q, is defined by,

$$q = -\rho D \frac{\partial h}{\partial x}, \tag{5.16}$$

where D is unity Lewis number diffusivity. A full derivation of this heat flux definition with a unity Lewis number is found in Turns [74].

5.1.4 Mixture Fraction Equation

Here $\eta = \xi$ (where ξ is mixture fraction) and Equation 5.2 becomes

$$\frac{\partial}{\partial t}\int_{\Omega(t)} \rho \xi dV = \frac{\partial}{\partial t}\int_{\hat{\Omega}(t)} \rho \xi dV + \int_{\hat{\Pi}} \rho \xi \vec{v}_R \cdot \vec{n} dA. \tag{5.17}$$

The system and control volume velocities are again defined as the gas mass average velocity and are equal, so $\vec{v}_R = 0$. Integrating over the control volume and rearranging gives

$$\frac{\partial \rho \xi \gamma \Delta x}{\partial t} = -(j_e - j_w) + S_\Phi \Delta x \gamma, \tag{5.18}$$

where j is the mixture fraction flux. By applying the definition of a derivative of products to the left side of the equation the equation becomes

$$\rho \gamma \Delta x \frac{\partial \xi}{\partial t} + \xi \frac{\partial \rho \gamma \Delta x}{\partial t} = -(j_e - j_w) + S_\phi \Delta x \gamma. \tag{5.19}$$

Substituting the mass conservation equation into the second term and rearranging the Lagrangian mixture fraction equation is

$$\frac{\partial \xi}{\partial t} = -\frac{j_e - j_w}{\rho \gamma \Delta x} + (1 - \xi)\frac{S_\Phi}{\rho}. \tag{5.20}$$

The mixture fraction flux, j, is defined by,

$$j = -\rho D \frac{\partial \xi}{\partial x}, \tag{5.21}$$

where D is unity Lewis number diffusivity.

5.2 Particle Modeling Method

Heterogeneous reactions in turbulent flow involve complex energy, mass, and chemical balances. This study uses simplified fuels and chemistry to reduce computational expense. Although the ODT model uses an adaptive grid, this would increase the complexity of the pyrolysis of stationary particles. Therefore the stationary particles are defined along a uniform grid, which is coupled to the adaptive gas phase grid. The particles are assumed spherical and are defined by a constant density, ρ_p. A number density n_p is used for a given cell, where n_p is constant throughout the simulation as it advances. Within each cell particles are taken to have the same volume, with total surface area A_p, throughout the cell (which by default defines the particle mass m_p in the cell volume). A void fraction γ is another variable to define a cell in the uniform wood particle grid. This is the same γ used in the gas phase reactions and is used to relate the two lines.

The cell sizes and locations across the ODT gas phase and wood grids are different. A couple of these properties must be exchanged across the grids to treat the two grids as a single system. The particle properties that are used in the gas phase include γ and S_Φ. These are coupled by a weighted sum method in which the following conservation equations are maintained:

$$\text{pyrolysis gas source: } \Delta x_g \gamma S_{\Phi,g} = \sum_i \Delta x_i \gamma_i \chi_i S_{\Phi,i} \tag{5.22}$$

and

$$\text{void fraction: } \gamma_g \Delta x_g = \sum_i \gamma_i \chi_i \Delta x_i, \tag{5.23}$$

where inherently $\Delta x_g = \sum_i \chi_i \Delta x_i$, χ is the fraction of the particle grid cell that overlaps the location of the gas phase cell, and the subscripts g and i refer to ODT gas phase grid and the uniform particle grid, respectively. This coupling is shown visually in Figure 5.1.

5.2.1 Mass and Energy Equations for the Particles

The mass and energy of the wood particles must evolve with the line as these properties dictate the source term for the gas phase reactions (S_Φ). The conservation equations of these properties and the equations relating them to the turbulent gas phase are detailed in this section.

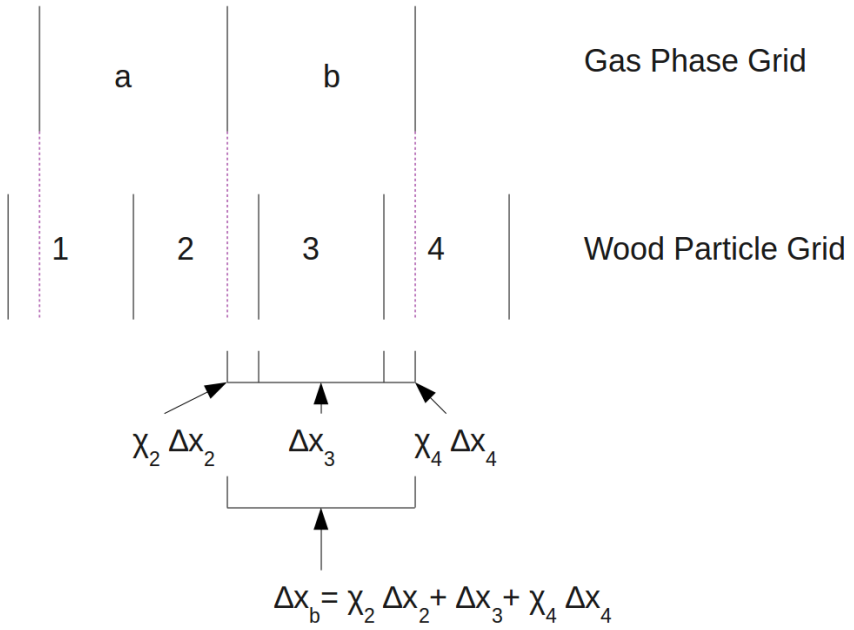

Figure 5.1: Visual illustration of the coupling of the gas phase and wood particle grid.

A simple mass balance equation is used to define the intensive mass (per unit volume) of the particles in a cell:

$$\frac{\partial m_p}{\partial t} = -\dot{y}_p \rho_p (1-\gamma), \tag{5.24}$$

where $\dot{y}_p$ is a yield rate of pyrolysis gas (mass fraction of off gas to total particle mass per second), which is defined in more detail later in the wood particle chemistry section. Then γ is tied algebraically to the mass so that:

$$\gamma = 1 - \frac{m_p}{\rho_p}. \tag{5.25}$$

The mass leaving the particle is the gas fuel source term (or amount of devolatilization gas leaving the particle), $S_\Phi = -\frac{\partial m_p}{\partial t}$.

In this first implementation, simplified heat transfer mechanisms were used. These assumptions can be relaxed in future studies. The heat transfer within the particles is assumed to be fast compared to the heat transfer to the particle, and a lumped capacitance method is employed. The heat of pyrolysis is considered small [75–77] and it is assumed that the fuel moisture does not affect the particle heat up (due to the low moisture content of excelsior fuels). Then the energy

balance across the particles in a cell is given by

$$\frac{\partial(m_p h_p)}{\partial t} = A_p \sigma \varepsilon (T_\infty - T_p) + A_p \theta h_c (T_\infty - T_p), \tag{5.26}$$

where h_p is the enthalpy of the particles, A_p is the surface area of the particles, σ is the Stephan-Boltzmann constant, ε is the particles emissivity (here the particles are treated as black bodies), h_c is the particles heat transfer coefficient, θ is the blowing factor that corrects for high mass transfer rates [78], T is the temperature, and the subscripts ∞ and p indicate surrounding air and particle, respectively. By applying the definition of the derivative of products to the left side of Equation 5.26 and rearranging, the energy balance can be used to solve directly for the enthalpy of the particles:

$$\frac{\partial h_p}{\partial t} = \frac{A_p}{m_p}(\sigma \varepsilon (T_\infty^4 - T_p^4) - h_c \theta (T_p - T_\infty)) - \frac{h_p}{m_p}\frac{\partial m_p}{\partial t}. \tag{5.27}$$

The surface area in this equation is given by

$$A_p = \pi D_p^2 n_p, \tag{5.28}$$

where D_p is the particle diameter and is calculated as a function of γ from the definition of the particle volume (V_p)

$$V_p = \frac{1}{6}\pi D_p^3 n_p = 1 - \gamma, \tag{5.29}$$

or

$$D_p = \left(\frac{1-\gamma}{\frac{1}{6}\pi n_p}\right)^{\frac{1}{3}}. \tag{5.30}$$

A Nusselt number (Nu) approach is used to calculate the average heat transfer coefficient. In this model Nu is calculated with the Ranz and Marshall [71] empirical formula

$$Nu = 2 + 0.6 Re^{\frac{1}{2}} Pr^{\frac{1}{3}}, \tag{5.31}$$

where Re and Pr are the Reynolds and Prandlt number evaluated with the local gas phase properties. T_p is calculated from h_p using the particle heat of formation and heat capacity.

Table 5.1: Kinetic parameters for the particle devolatilization model.

Symbol	Parameter	Value
y_p^* (wt% of total particle mass)	Ultimate Yield	92.97
k_0 (1/s)	Kinetic Pre-exponential Factor	33884
E (kcal/mol)	Activation Energy	16.5

5.2.2 Wood Particle Chemistry

There are two chemical processes going on in this wood particle simulation: (1) wood pyrolysis and (2) combustion of the pyrolysis gases. These are both very complex processes involving complex chemical systems. This model uses simplified models of both processes. Here the particles are treated as sweet gum hardwood. This wood has been initially implemented, because not many single-reaction, first order, kinetic parameters are available for other wood types.

Wood Pyrolysis

An empirical, single-reaction, first order devolatilization model [73] was used in this work to obtain the pyrolysis off-gas yield rate. This kinetic model is ubiquitous in the thermal analysis of the particles, therefore the gas phase temperature is used rather than particle temperature. This form has been successfully used to model the devolatilization of both wood and other solid fuels [79–83]. In this model the rate of total volatile yield is given by

$$\dot{y}_p = \frac{\partial y_p}{\partial t} = (y_p^* - y_p) k_0 e^{-\frac{E}{RT_p}}, \tag{5.32}$$

where y_p is the volatile yield, T_p is the particle temperature of the cell, and R is the ideal gas constant. Here y_p^*, k, and E are kinetic parameters defined in Table 5.1 for the sweet gum wood.

Pyrolysis Off-gas Combustion

A pyrolysis off-gas mixture fraction approach was employed for this case with an equilibrium look-up table. This approach is described further in the look-up table chemistry section in

Chapter 3. It was also assumed that the composition of the pyrolysis off-gas of the particles is constant throughout the simulation. This way the look-up table requires a single mixture fraction ξ, rather than multiple mixture fractions. For example, if moisture and devolatilization were treated separately than they would have different rates and each would need a separate mixture fraction. The elemental composition of the pyrolysis products was assumed to be the same as that of the wood particles ($C_{32}H_{46}O_{21}$). Since the equilibrium software used in our code [57] requires chemical compounds rather than elements, a surrogate gas was chosen to be equilibrated with varying air levels (based on mixture fraction). This surrogate gas was assumed to be H_2O, CO_2, and C_6H_6, where the mole fractions of these compounds were calculated by an elemental balance with composition of the wood and are summarized in Table 5.2.

Table 5.2: Chemical composition of the surrogate fuel.

Compound	Mole Fraction
H_2O (g)	0.495
CO_2	0.283
C_6H_6	0.222

The surrogate gas temperature was calculated so that the gas had the same enthalpy as the wood at standard conditions (i.e. the heat of formation of the wood $H_{f,wood}$). $H_{f,wood}$ was calculated from the heat of combustion of the wood ΔH_c (8450 BTU/lb) [73]. This was done by applying the definition of ΔH_c,

$$\Delta H_c = H_{reactants} - H_{products}, \tag{5.33}$$

to the wood combustion reaction:

$$C_{32}H_{46}O_{21} + 37O_2 \longrightarrow 36CO_2 + 23H_2O. \tag{5.34}$$

In this calculation $H_{reactants} = H_{f,wood}$ (because the heat of formation of oxygen is zero) and $H_{products} = 36H_{f,CO_2} + 23H_{f,H_2O}$. These definitions were substituted into Eq. 5.33 and then the

equation was rearanged giving

$$H_{f,wood} = \Delta H_c + 36H_{f,CO_2} + 23H_{f,H_2O}. \tag{5.35}$$

H_{f,CO_2} and H_{f,H_2O} values were taken from [74]. The value of $H_{f,wood}$ was calculated to be -4.1E6 J/mol or -5.3E6 J/kg. From this the temperature of the surrogate gas was determined using the Gaseq software package [84] and found to be 411 K.

5.3 Evolution Procedure

The solution procedure for the solid particle code follows a similar evolution procedure as the temporal and spatial formulations described in Chapter 3, but includes extra steps to evolve and couple both the particle and gas phase lines. The set of ordinary differential equations are solved using an explicit Euler method. As in Chapter 3, the first order Euler method is described here, but a second order method is also included in the ODT code. The algorithm for solution of the ODT with solid fuel particles is as follows:

1. Initialize velocity, enthalpy, species, and particle profiles.

2. Couple γ and S_Φ values in the gas phase (the adaptive grid) and wood line , using the appropriate conservation equations (Equations 5.22 and 5.23).

3. Compute mass, heat, and momentum fluxes, along with reaction source terms in the gas phase.

4. Use gas phase and particle properties to calculate the devolatilization rate for the particle line (Equation 5.32).

5. Advance both the particle and gas phase lines with the same time step using Equations 5.24, 5.25 5.27, 5.9, 5.15, and 5.20). This yields the particle and gas phase evolved properties for a single time step.

6. Get the auxiliary gas phase variables (such as temperature, density, and species composition) from the look-up table.

7. Update the grid size, Δx, for all the cells in the gas phase grid.

8. Steps 2-7 are then repeated until the diffusion is completed.

5.4 Results for a Preliminary Case

This particle code was implemented for future simulations of solid fuel beds. Here a simple preliminary case was run in which a cluster of stationary wood particles of diameter 3 cm were pyrolyzed and evolved temporally. These particles were assumed to be evenly spaced throughout the particle cluster. The particle cluster was set with a length of 6 m, while the simulation was performed on a ODT domain of 10 meters. The velocity and mixture fraction profiles were initialized as a jet with hyperbolic tangent transitions. The void volume fraction (fraction of gas phase to particles) was initialized as a simple step function with a value of one (all gas phase) at the edges and 0.5 at the center. The initial temperature profile was set by equilibrating the initial mixture fraction profile. These initial profiles are shown in Figure 5.2. The wood line cells were given a particle number density of 1000 m^{-3} and the wood particle density was set as 500 $\frac{kg}{m^3}$. In this case 128 realizations were used to calculate the statistics. The simulation was performed at the Fulton Super Computing Laboratory at Brigham Young University. The simulation required approximately 20 CPU-hours on 2.8 GHz Intel Nehalem processors. The following ODT parameters were used in all simulations: C=8, Z=1000, and β=0.7 (the same as those used for the ethylene fire wall). A two-flux radiation model, detailed in Chapter 3, was used. Buoyancy effects were not included in this simulation.

The gas phase temperature profiles are shown in Fig. 5.4. The two peaks in the early mean temperature profiles were due to the initial temperature profile and smoothed together after the particles began to react. The temperature peaks affected particle heat-up, and the particle mean temperature and devolatilization yield profiles also exhibited two peaks in the first 40 seconds of the simulation. The root mean square (RMS) temperature profile also exhibited two peaks, but, in contrast to the mean temperature profile, the peaks remained throughout the entire simulation. The fluctuations were large in the beginning of the simulation as the initial profile introduced large gradients and therefore more turbulent mixing. The RMS fluctuations decreased in time and then began to increase as the particles devolatized. The two RMS fluctuation peaks are located at the

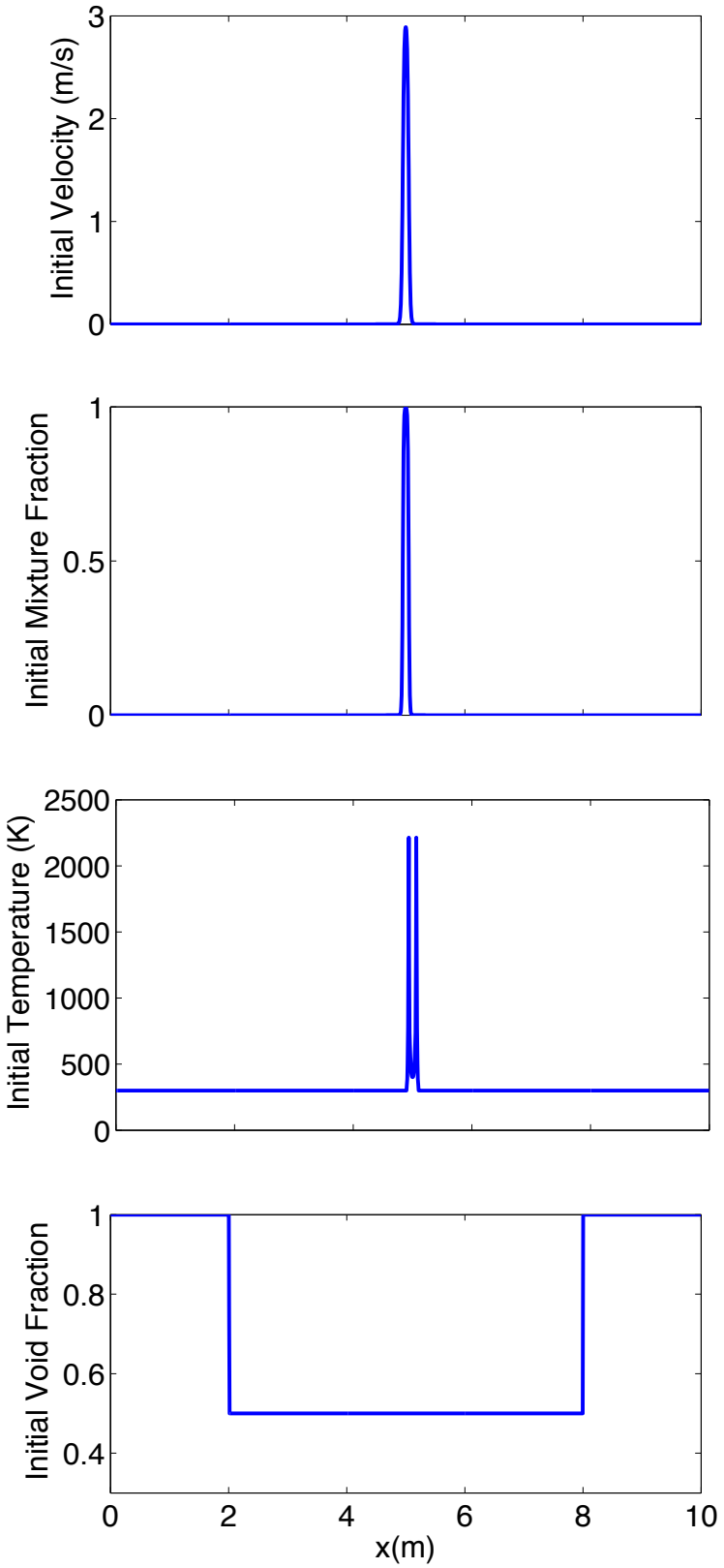

Figure 5.2: Initial profiles of velocity, mixture fraction, temperature and void fraction (γ).

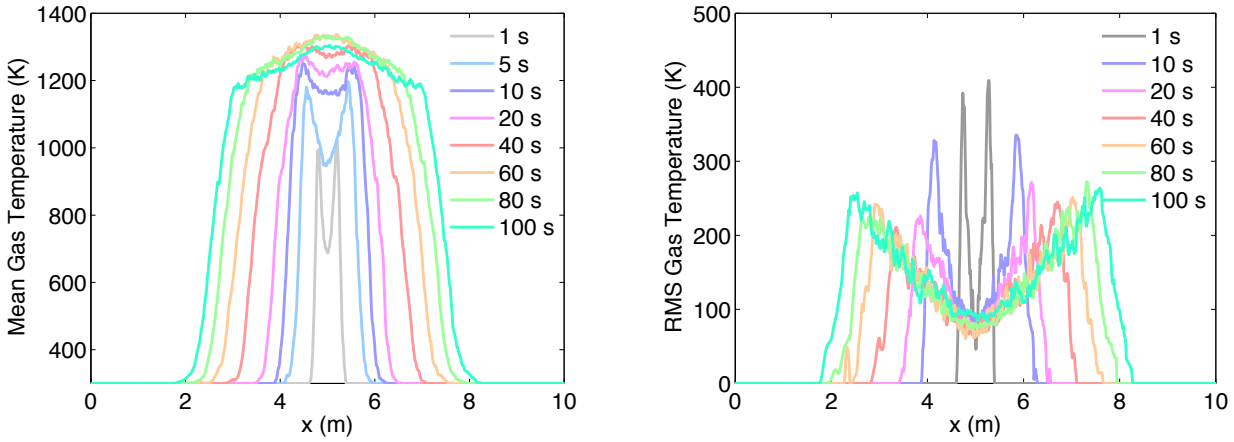

Figure 5.3: Mean and RMS profiles of gas phase temperature.

edge of the devolatilization zone, where the flame front is most intermittent. Both the mean and RMS temperature profiles spread with time.

Figure 5.4 shows the mean and root mean square fluctuations (RMS) of particle temperature and devolatilization yield. The mean particle temperatures increase to a peak of approximately 1300 K (which is also the temperature of the gas phase) and then remain at that temperature. The width of the profile increases linearly with time. The RMS temperature profile of the particles has two peaks at the edges of the devolatizing particle zone, because of the turbulent nature of the flame front at that location. The particles heat up intermittently due to the turbulence. The mean volatile yield of the particles increases with time to the ultimate yield of 0.93, given in the kinetic model. The the devolatilization zone spreads linearly after this ultimate yield has been reached. Devolatilization of the particles did not begin until after 10 seconds of exposure to the jet flame, which is when the particles were heated to a temperature of about 500 K. The particle RMS volatile yield peaks at the edges of the devolatilization zone where the devolatilization rates are the greatest. The fluctuations increase with time as the flame front becomes more turbulent and particle heat-up becomes more intermittent.

5.5 Summary

Solid fuel particles were incorporated into the ODT model to to provide a means of simulating this convective heating of unburnt fuel through direct flame contact. The mechanics of this

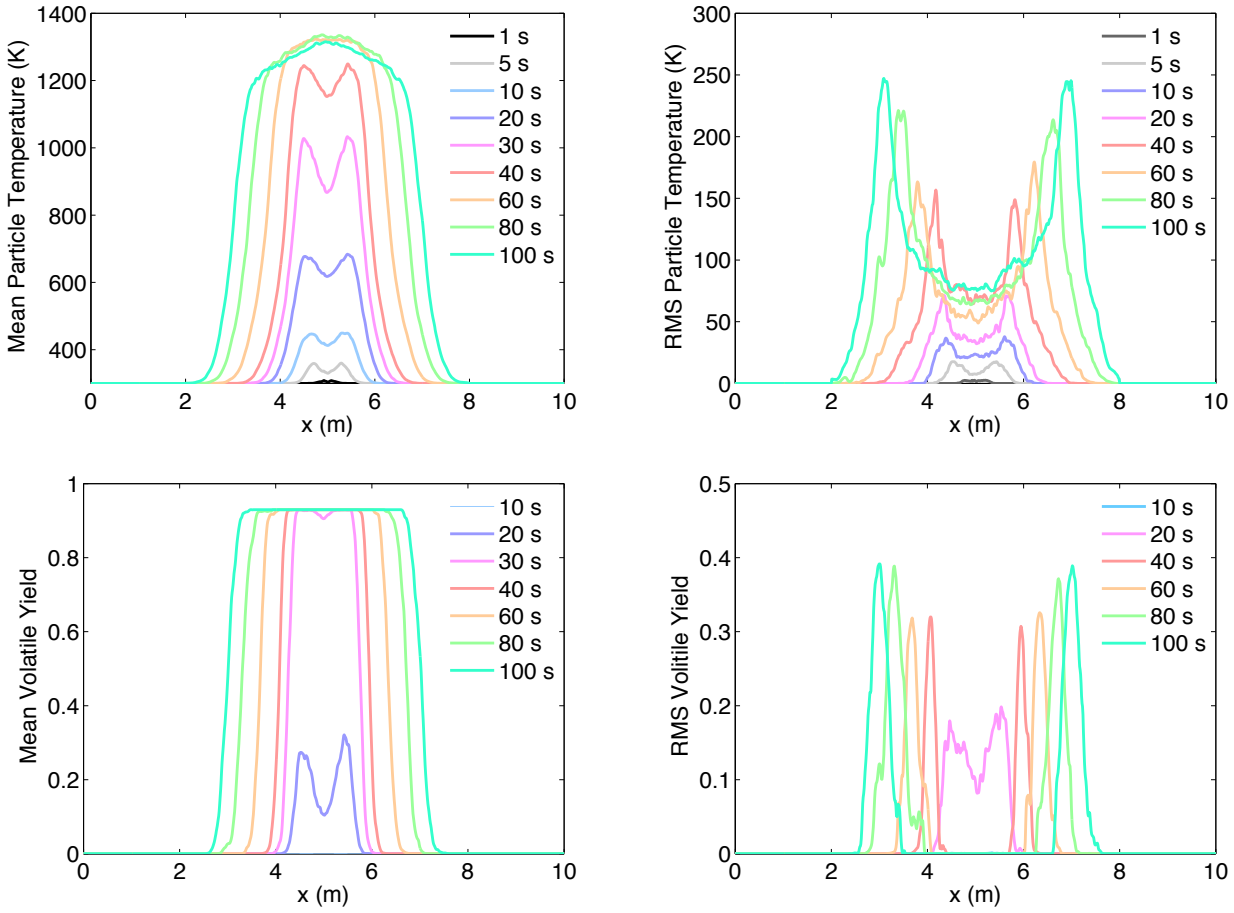

Figure 5.4: Mean and RMS profiles for temperature and volatile yield.

particle code were implemented in a more general manner, so that it can be used in a broad range of simulations. The code can easily be adapted to more complicated fuel configurations, kinetic models, and heat transfer mechanisms. Here, a simple case was presented where a cluster of stationary wood particles were pyrolyzed over a short time. Preliminary results were presented for this simple case. This implementation is the first step toward the simulation of a solid fuel bed.

CHAPTER 6. CONCLUSIONS AND FUTURE WORK

This thesis discusses the application of the ODT model to the study of flame propagation by direct flame bathing in lab-scale fires to study phenomena of interest to wildland fires. The following contributions were made in these efforts:

1. A spatial formulation of ODT was formulated and implemented.

2. An ethylene wall fire was simulated to gain knowledge of a flame front.

3. Solid wood particle devolatilization was implemented into the ODT code.

This chapter presents a summary of the conclusions and results of this research. This work extends the application of the ODT model to the study of fire spread research and provides a new, relatively economical tool for modeling the turbulent nature in these fires.

6.1 Spatial ODT Code

As one of the primary interests of this research is to capture the intermittent and turbulent nature of a flame front, the correct tools were needed to study these kinds of fires. A spatial formulation of ODT was developed from the existing temporal ODT code to meet this need. This spatial code was validated by simulations of an isothermal heated wall. These simulations showed good agreement with experimental data. The main conclusion of this validation was that the spatial formulation of ODT is able to capture key features of a buoyant, turbulent flow.

6.2 Ethylene Wall Fire Simulations

Ethylene wall flame simulations were performed to provided insight into the intermittent behavior of a turbulent flame front. Simulations were performed at three flow rates: 235, 390, and 470 L/min. Peak mean temperatures for all flow rates were near 1550 K and the temperature

profiles spread with increasing flow rate. Maximum mean velocities increased with increasing flow rate. The peak mean velocities were predicted to range from 6-6.5 m/s. The velocity profiles did not spread with increasing flow rate. The velocity profiles were self similar when scaled by the max velocity and the width of the profile at half the maximum velocity. This is consistent with wall fire literature [56, 70]. Comparison with experimental temperature results showed generally good agreement, though temperatures were under-predicted by up to 15% of experiments in the flame zone, and temperature fluctuations were over-predicted. All major trends were captured in the simulations.

Results of particular interest in flame propagation are fluctuating temperature field statistics. The power spectral density (PSD) of temperature in the time domain was computed and was proportional to $f^{-5/3}$ in the integral region. Probability profiles of temperatures greater than 600 K and 1000 K were also predicted. These probability profiles were wider at the top of the wall than near the base. These profiles show temperatures greater than 1000 K reach 15 cm from the wall at a height of 1.8 m. Full temperature probability density functions (PDFs) were computed at the top of the flame wall. The PDFs shift to lower temperatures and become more narrow with increasing distance from the wall. The two PDFs furthest from the wall were bimodal due to the significant amounts of ambient air being entrained. This indicates the extent of the intermittent behavior of the flame front. The ODT model can capture the intermittent nature of the flame front.

6.3 Solid Fuel Devolatilization

Solid fuel particles were incorporated into the ODT model to provide a means of simulating this convective heating of unburnt fuel through direct flame contact. A simple case was run in which a cluster of stationary wood particles were pyrolyzed starting with a narrow, initial temperature profile at the center of the domain. Pyrolysis did not occur until after the particles reached a temperature greater than 500 K. Particle temperature profile width increased linearly with time and the devolatilization yield profiles mirrored this behavior. The RMS temperature and volatile yield profiles exhibited two peaks at the outer edges of the reacting zone. This was due to the higher devolatilization rates and intermittent flame front behavior. While only preliminary results were presented for this simple case, this extension of the ODT model to the pyrolysis of solid wood particles presents new opportunities for future research.

6.4 Areas for Future Work

The primary objectives of this work were: (1) to increase understanding of flame structure and important statistics that describe a flame front, and (2) present ODT as a viable tool in understanding flame propagation in fuel beds. This is the first time the ODT has been extended to the study of flame propagation in fuel beds, and there are many opportunities for future work and development. Some of these are listed in this section.

6.4.1 Incorporation of Variable Fuels

In this thesis the solid particles are treated as devolatilizing spheres, with a simple single-reaction, first order chemistry model. A more complex fuel array definition would allow for better representation of a solid fuel bed fire. Treating the fuels as cylinders or a more complex configuration might better represent an actual fuel bed. This would require different equations for heat transfer coefficients, volumes, etc. Also, a more complex particle chemistry model might provide more accurate devolatilization rates and gas compositions. As well, this model could be extended to include the heterogeneous char combustion of these particles. An interesting study would treat the particle chemistry with a single particle model rather than a global model.

6.4.2 Incorporation of Wind

Wildland fire propagation is greatly affected by wind. The intermittency of a flame front is changed when a cross wind is present. Incorporation of a cross flow into the ODT simulation would be beneficial in understanding the effects of wind on the structure and statistics of a flame front. Both laminar and turbulent cross-flows would be of interest in this case. A possible method for incorporation of a laminar cross flow is by having the ODT domain move with the velocity of the cross flow, while keeping the fuel source stationary.

6.4.3 Application of ODT to Particle Solid Fuel Fires

The studies done in this thesis modeled a flame front and incorporated solid fuels. These are both steps to better understand flame propagation by direct flame contact. However, validation

of the solid particle fuel code is needed. This could be done for a single particle or for a more complex configuration.

Application of the ODT model to an actual fuel bed fire would provide further understanding of the turbulent structure of a flame front within a fuel bed. Experimental data are available for these kinds of fires. These simulations would demonstrate the ability of ODT to capture flame propagation via flame bathing. It would also determine the feasibility of extending the ODT model to capture even larger and more complex fires (such as an actual wildland fire).

REFERENCES

[1] Beer, T., 1990. "The iteraction of wind and fire." *Boundary-Layer Meteorology,* **54**, pp. 287–308.

[2] Albini, F., 1985. "A model for fire spread in wildland fuels by radiation." *Combustion Science and Technology,* **42**, pp. 229–258.

[3] Albini, F., 1996. "Iterative solution of the radiation transport equations governing spread of fire in wildland fuel." *Combustion, Explosion, and Shock Waves,* **32**, pp. 534–542.

[4] Butler, B., Finney, M., Andrews, P., and Albini, F., 2004. "A radiation-driven model for crown fire spread." *Canadian Journal of Forest Research,* **34**, pp. 1588–1599.

[5] Finney, M., Jimenez, D., Cohen, J., Grenfell, I., and Wold, C., 2010. "Structure of diffusion flames from a vertical burner." In *VI International Conference on Forest Fire Research*.

[6] Weber, R., 1991. "Modelling fire spread through fuel beds." *Progress in Energy Combustion Science,* **17**, pp. 67–82.

[7] Cohen, J., and Finney, M., 2010. "An examination of fuel particle heating during fire spread." In *VI International Conference on Forest Fire Research*.

[8] Pitts, W., 1991. "Wind effects on fires." *Progress in Energy and Combustion Science,* **17**, pp. 83–134.

[9] Yedinak, K., Cohen, J. D., Forthofer, J., and Finney, M., 2010. "An examination of flame shape related to convection heat transfer in deep-fuel beds." *International Journal of Wildland Fire,* **19**, pp. 171–178.

[10] Kerstein, A. R., 1999. "One-dimensional turbulence: model formulation and application to homogeneous turbulence, shear flows, and buoyant stratified flows." *J. Fluid Mech.,* **392**, pp. 277–334.

[11] Kerstein, A. R., Ashurst, W. T., Wunsch, S., and Nilsen, V., 2001. "One-dimensional turbulence: vector formulation and application to free shear flows." *Journal of Fluid Mechanics,* **447**, pp. 85–109.

[12] Wilcox, D., 2006. *Turbulence Modelling for CFD*., 3 ed. DCW Industries Inc.

[13] Hilbert, R., Tap, F., el Rabii, H., and Thevenin, D., 2004. "Impact of detailed chemistry and transport models on turbulent combustion simulations." *Progress in Energy and Combustion Science,* **30**, pp. 61–117.

[14] Porterie, B., Morvan, D., Larini, M., and Loraud, J., 1998. "Wildfire propagation: a two-dimensional miultiphase approach." *Combustion, Explosion, and Shock Waves,* **34**, pp. 139–150.

[15] Larini, M., Giroud, B., Porterie, B., and Loraud, J. C., 1998. "Multiphase formulation for fire propagation in heterogeneous combustible media." *International Journal of Hear and Mass Transfer,* **41**, pp. 881–897.

[16] Porterie, B., Morvan, D., Loraud, J. C., and Larini, M., 2000. "Firespread through fuel beds: Modeling of wind-aided fires and induced hydrodynamics." *Physics of Fluids,* **12**, pp. 1762–1782.

[17] Morvan, D., and Dupuy, J., 2001. "Modeling of fire spread through forest fuel bed using a multiphase formulation." *Combustion and Flame,* **127**, pp. 1981–1994.

[18] Linn, R., 1997. "A transport model for prediction of wildfire behavior." PhD thesis, New Mexico State University.

[19] Linn, R., Rieisner, J., Colman, J., and Winterkamp, J., 2002. "Studying wildfire behavior using firetec." *International Journal of Wildland Fire,* **11**, pp. 233–246.

[20] Morvan, D., and Larini, M., 2001. "Modeling of one dimensional fire spread in pine needles with opposing air flow." *Combustion Science and Technology,* **164**, pp. 37–64.

[21] Kennedy, L. A., and Plumb, O. A., 1976. "Prediction of bouyancy controlled turbulent wall diffusion flames." *Proc. Combust. Inst.*, pp. 1699–1707.

[22] Tamanini, F., 1979. "A numerical model for the prediction of radiation-controlled turbulent wall fires." *Proc. Combust. Inst.,* **17**, pp. 1075–1085.

[23] Joulain, P., 1996. "Convective and radiative transport in pool and wall fires: 20 years of research in pointiers." *Fire Safety Journal,* **26**, pp. 99–149.

[24] Pitsch, H., 2006. "Large-eddy simulation of turbulent combustion." *Annual Review of Fluid Mechanics,* **38**, pp. 453–482.

[25] Zhou, X., Mahalingam, S., and Weise, D., 2007. "Experimental study and large eddy simulation of terrain slope on marginal burning in shrub fuel beds." *Proc. Combust. Inst.,* **31**, pp. 2547–2555.

[26] Wang, H., Coutin, M., and Most, J., 2002. "Large-eddy-simulation of buoyancy-driven fire propagation behind a pyrolysis zone along a vertical wall." *Fire Safety Journal,* **37**, pp. 259–284.

[27] Chen, J. H., Choudhary, A., de Supinski, B., DeVries, M., Hawkes, E. R., Klasky, S., Liao, W. K., Ma, K. L., Mellor-Crummey, J., Podhorszki, N., Sankaran, R., Shende, S., and Yoo, C. S., 2009. "Terascale direct numerical simulations of turbulent combustion using S3D." *Computational Science and Discovery,* **2**, pp. 1–31.

[28] Kerstein, A. R., 1988. "A linear-eddy model of turbulent scalar transport and mixing." *Combustion Science and Technology,* **60**, pp. 391–421.

[29] Kerstein, A., 1990. "Linear-eddy modelling of turbulent transport: part 3. mixing and differential molecular diffusion in round jets." *Journal of Fluid Mechanics,* **216**, pp. 411–435.

[30] Kerstein, A., 1991. "Linear-eddy modelling of turbulent transport: part 6. microstructure of diffusive scalar mixing fields." *Journal of Fluid Dynamics,* **231**, pp. 361–394.

[31] Kerstein, A., 1992. "Linear-eddy modeling of turbulent transport: part 4. structure of diffusions flames." *Journal of Fluid Dynamics,* **240**, p. 289.

[32] Ashurst, W. T., Kerstein, A. R., Pickett, L. M., and Ghandhi, J. B., 2003. "Passive scalar mixing in a spatially developing shear layer: Comparison of one-dimensional turbulence simulations with experimental results." *Physics of Fluids,* **15**, pp. 579–582.

[33] Ashurst, W. T., and Kerstein, A. R., 2005. "One-dimensional turbulence: variable density formulation and application to mixing layers." *Phys. Fluids,* **17-025107**, pp. 1–26.

[34] Schmidt, R. C., Kerstein, A. R., Wunsch, S., and Nilsen, V., 2003. "Near-wall LES closure based on one-dimensional turbulence modeling." *Journal of Computational Physics,* **186**, pp. 317–355.

[35] Cao, S., and Echekki, T., 2008. "A low-dimensional stochastic closure model for combustion large-eddy simulation." *Journal of Turbulence,* **9**, pp. 1–35.

[36] Schmidt, R. C., Kerstein, A. R., and McDermott, R., 2010. "ODTLES: a multi-scale model for 3D turbulent flow based on one-dimensional turbulence modeling." *Comput. Methods Appl. Mech. Engrg.,* **199**, pp. 865–880.

[37] Schmidt, J., Wendt, J., and Kerstein, A., 2009. "Non-equilibrium wall deposition of inertial particles in turbulent flow." *J. Strat. Phys.,* **137**, pp. 233–257.

[38] Dreeben, T. D., and Kerstein, A. R., 2000. "Simulation of vertical slot convection using one-dimensional turbulence." *International Journal of Heat and Mass Transfer,* **43**, pp. 3823–3834.

[39] Shihn, H., and DesJardin, P. E., 2007. "Near-wall modeling of an isothermal vertical wall using one-dimensional turbulence." *International Journal of Heat and Mass Transfer,* **50**, pp. 1314–1327.

[40] Echekki, T., Kerstein, A. R., and Dreeben, T. D., 2001. "One-dimensional turbulence simulation of turbulent jet diffusion flames: model formulation and illustrative applications." *Combustion and Flame,* **125**, pp. 1083–1105.

[41] Echekki, T., and Gupta, K., 2009. "Hydrogen autoignition in a turbulent jet with preheated co-flow air." *International Journal of Hydrogen Energy,* **34**, pp. 8352–8377.

[42] Hewson, J. C., and Kerstein, A. R., 2002. "Local extinction and reignition in nonpremixed turbulent $CO/H_2/N_2$ jet flames.." *Combustion Science and Technology,* **174**, pp. 35–66.

[43] Ranganath, B., and Echekki, T., 2008. "One-dimensional turbulence-based closure with extinction and reignition." *Combustion and Flame,* **154**, pp. 23–46.

[44] Ranganath, B., and Echekki, T., 2009. "Odt closure with extinction and reignition in piloted methane-air jet diffusion flames." *Combustion Science and Technology,* **181**, pp. 570–596.

[45] Ricks, A. J., Hewson, J. C., Kerstein, A. R., Gore, J. P., Tieszen, S. R., and Ashurst, W. T., 2010. "A spatially developing one-dimensional turbulence (ODT) study of soot and enthalpy evolution in meter-scale buoyant turbulent flames." *Combust. Sci. Technol.,* **182**, pp. 60–101.

[46] Shihn, H., and DesJardin, P. E., November 13-20, 2004. "Near-wall modeling for vertical wall fires using one-dimensional turbulence." In *Proceedings of IMECE04 ASME International Mechanical Engineering Congress and Exposition, Anaheim, CA*.

[47] DeRis, J., and Orloff, L., 1975. "The role of bouyancy direction and radiation in turbulent diffusion flames on surfaces." *Proc. Combust. Inst.,* **15**, pp. 175–182.

[48] Orloff, L., 1975. "Upward turbulent fire spread and burning of fuel surfaces." *Proc. Combust. Inst.,* **15**, pp. 183–192.

[49] Orloff, L., Modak, A., and Alpert, R., 1977. "Burning of large-scale vertical surfaces." *Proc. Combust. Inst.,* **16**, pp. 1345–1354.

[50] King-Mon, T., and Quimtiere, J., 1991. "Wall flame heights with external radiation." *Fire Technology,* **27**, pp. 195–203.

[51] Markstein, G. H., and Ris, J. D., 1992. "Wall-fire radiant emission–part 2: radiation and heat transfer from porous-metal wall burner flames." *Proc. Combust. Inst.,* **24**, pp. 1747–1752.

[52] Quintiere, J., 1981. "An approach to modeling wall fire spread in a room." *Fire Safety Journal,* **3**, pp. 201–214.

[53] Mitler, H., 1990. "Predicting the spread reates of fires on vertical surfaces." *Proc. Combust. Inst.,* **23**, pp. 1715–1721.

[54] Delichatsios, M., 1982. "Turbulent convective flows and burning on vertical walls." *Proc. Combust. Inst.,* **19**, pp. 855–868.

[55] Delichatsios, M. A., 1984. "Flame heights in turbulent wall fires with significant flame radiation." *Combustion Science and Technology,* **39**, pp. 195–214.

[56] Delichatsios, M. A., 1986. "A simple algebraic model for turbulent wall fires." *Proceedings of the Combustion Institute,* **21**, pp. 53–64.

[57] Goodwin, D., 2011. Cantera, an object-oriented software toolkit for chemical kinetics, thermodynamics, and transport processes `http://code.google.com/p/cantera`.

[58] McDermott, R. J., 2005. "Toward one-dimensional turbulence subgrid closure for large-eddy simulation." PhD thesis, The University of Utah.

[59] Tsuji, T., and Nagano, Y., 1989. "Velocity and temperature measurements in a natural convection boundary layer along a vertical flat plate." *Experimental Thermal and Fluid Science,* **2**, pp. 208–215.

[60] Westbrook, C. K., and Dryer, F. L., 1981. "Simplified reaction mechanisms for the oxidation of hydrocarbon fuels in flames." *Combustion Science and Technology,* **27**, pp. 31–43.

[61] Lignell, D. O., Chen, J. H., Smith, P. J., Lu, T., and Law, C. K., 2007. "The effect of flame structure on soot formation and transport in turbulent nonpremixed flames using direct numerical simulation." *Combustion and Flame,* **151**, pp. 2–28.

[62] Qin, Z., Lissianski, V. V., Yang, H., Gardiner, W. C., Davis, S. G., and Wang, H., 2000. "Combustion chemistry of propane: a case study of detailed reaction mechanism optimization." *Proceedings of the Combustion Institute,* **28**, pp. 1663–1669.

[63] Kee, R. J., Rupley, F. M., and Miller, J. A., 2000. *Chemkin*. Reaction Design, Inc., San Diego CA.

[64] Cohen, S., and Hindmarsh, A., 1996. "CVODE, a stiff/nonstiff ODE solver in C." *Comput. Phys.,* **10**, pp. 138–143 `http://llnl.gov/casc/sundials/`.

[65] Peters, N., 1984. "Laminar diffusion flamelet models in non-premixed turbulent combustion." *Progress in Energy and Combustion Science,* **10**, pp. 319–339.

[66] Modest, M. F., 1993. *Radiative Heat Transfer*. McGraw-Hill, New York.

[67] Ju, Y., Guo, H., Maruta, K., and Liu, F., 1997. "On the extinction limit and flammability limit of non-adiabatic stretched methaneair premixed flames." *Journal of Fluid Mechanics,* **342**, pp. 315–334.

[68] Leung, K. M., and Lindstedt, R. P., 1991. "A simplified reaction mechanism for soot formation in nonpremixed flames." *Combustion and Flame,* **87**, pp. 289–305.

[69] Incropera, F., and DeWitt, D., 1996. *Fundamentals of Heat and Mass Transfer*. John Wiley and Sons, New York.

[70] Ahmad, T., and Faeth, G. M., 1979. "Turbulent wall fires." *Proceedings of the Combustion Institute,* **17**, pp. 1149–1160.

[71] Ranz, W. E., and Marshall, W. R., 1952. "Evaporation from drops." *Chemical Engineering Progress,* **48**, pp. 173–180.

[72] Ragland, K., Aerts, D., and Baker, A., 1991. "Properties of wood for combustion analysis." *Bioresource Technology,* **37**, pp. 161–168.

[73] Nunn, T., Howard, J., Longwell, J., and Peters, W., 1985. "Product compositions and kinetics in the rapid pyrolysis of sweet gum hardwood." *Ind. Eng. Chem. Process Des. Dev.,* **24**, pp. 836–844.

[74] Turns, S. R., 2000. *An Introduction to Combustion*., 2nd ed. McGraw-Hill, New York.

[75] Gomez-Barea, A., Nilsson, S., Barrero, F., and Campoy, M., 2010. "Devolitilization of wood and wastes in fluidized bed." *Fuel Processing Technology,* **91**, pp. 1624–1633.

[76] Scott, S., Davidson, J., Dennis, J., and Hayhurst, A., 2007. "The devolatilization of part of a complex fuel (dried sewage sludge) in a fluidized beds." *Progress in Energy and Combustion Science,* **62**, pp. 584–598.

[77] Pyle, D., and Zaror, C., 1984. "Heat transfer kinetics in low temperature pyrolysis of solids." *Chemical Engineering Science,* **39**, pp. 147–158.

[78] Bird, R. B., Stewart, W. E., and Lightfoot, E. N., 2002. *Transport Phenomena.*, 2 ed. John Wiley and Sons.

[79] Franklin, H., Peters, W., Carlello, F., and Howard, J. B., 1981. "Effects of calcium minerals on the rapid pyrolysis ofa bituminous coal." *Ind. Eng. Chem. Process Des. Dev.,* **20**, pp. 670–674.

[80] Hajaligol, M., Howard, J. B., Longwell, J., and Peters, W., 1982. "Product compositions and kinetics for rapid pyrolysis of cellulose." *Ind. Eng. Chem. Process Des. Dev.,* **21**, pp. 457–466.

[81] Gronli, M., Varhegyi, G., and DiBlasi, C., 2002. "Thermogravimetric analysis and devolitilization kinetics of wood." *Ind. Eng. Chem. Res.,* **41**, pp. 4201–4208.

[82] Branca, C., Albano, A., and DiBlasi, C., 2005. "Critical evaluation of global mechanisms of wood devolitilization." *Thermochimica Acta,* **429**, pp. 133–141.

[83] Radmanesh, R., Courbariaux, Y., Chaouki, J., and Guy, C., 2006. "A unified lumped approach in kinetic modeling of biomass pyrolysis." *Fuel,* **85**, pp. 1211–1220.

[84] Morley, C., 2005. Gaseq, a chemical equilibrium program for windows `http://www.c.morley.dsl.pipex.com/`.